

---

## In situ record of sedimentary processes near the Rhône River mouth during winter events (Gulf of Lions, Mediterranean Sea)

C. Marion<sup>a, b, \*</sup>, F. Dufois<sup>b, c</sup>, M. Arnaud<sup>b</sup> and C. Vella<sup>d</sup>

<sup>a</sup> University of Perpignan, 52 Avenue Paul Alduy, 66860 Perpignan Cedex, France

<sup>b</sup> IRSN, DEI/SESURE Centre Ifremer, BP 330, 83507 La Seyne-sur-Mer, France

<sup>c</sup> IFREMER, Centre de Brest, BP 70, 29280 Plouzané, France

<sup>d</sup> CEREGE, Europôle de l'Arbois, BP 80, 13545 Aix-en-Provence Cedex 04, France

\*: Corresponding author : C. Marion, Tel.: +33 667110893, email address : [cedric.marion83@gmail.com](mailto:cedric.marion83@gmail.com)

---

### Abstract:

The environment is impacted by natural and anthropogenic disturbances that occur at different spatial and temporal scales, and that lead to major changes and even disequilibria when exceeding the resiliency capacities of the ecosystem. With an annual mean flow of 1700 m<sup>3</sup> s<sup>-1</sup>, the Rhône River is the largest of the western Mediterranean basin. Its annual solid discharges vary between 2 and 20 Mt, with flood events responsible for more than 70% of these amounts.

In the marine coastal area, close to the mouth, both flocculation and aggregation lead to the formation of fine-grained deposits, i.e. the prodelta. This area is characterized by sediment accumulation rates up to 20–50 cm yr<sup>-1</sup> and high accumulations of particle reactive contaminants such as various man-made radionuclides released into the river by nuclear facilities or arising from prior atmospheric nuclear tests (1954–1980) and the Chernobyl accident (April 1986). This prodelta, however, cannot be considered as a permanent repository for particle reactive pollutants since it is subjected to reworking processes.

Sediment dynamics had to be linked to the influences of hydrodynamic and atmospheric events such as high flow rates or storms close to the Rhône River mouth. An experiment was carried out during the winter 2006 based on the deployment of two ADCPs and six altimeters at the Grand Rhône mouth for several months. This type of installation has never been used before in this area because of the hard meteorological conditions and the strong fishing activities. However, results showed pluricentimetric rises of the sedimentary level just after river flood events and decreases during storms, generated by southeast winds. Radiotracers and grain size depth profiles helped to characterise the studied events and to establish inventories of sediments and radionuclides. A cruise (CARMEX) was carried out during this same period to collect water samples, suspended particles and sediment cores. The results enabled us to link both river flow and wind characteristics to events recorded on the sea floor, i.e. resuspension, accumulation, consolidation, etc. Deposits of 11 cm of sediments were estimated during flood periods and bottom shear stresses up to 5 N m<sup>-2</sup> were calculated during sediment erosion phases.

**Keywords:** Sediment dynamics; Floods; Hydrodynamics; Radiotracers; Rhône River prodelta

## 1. Introduction

Sediment dynamics in the Gulf of Lions have been studied in the framework of various projects (Ecomarge, Euromarge, Mater, US-Eurostrataform and EU-Eurostrataform (Monaco et al., 1990; Weaver et al., 2006)). These projects have led to a better understanding of sediment pathways from their sources, i.e. rivers, to their deposits in deltas, shelves, canyons and eventually to deep basins (Heussner et al., 2006; Palanques et al., 2006). The Gulf of Lions is especially interesting since it is a river-dominated continental shelf fed primarily by the Rhône River and also by several coastal rivers such as the Vidourle, Lez, Herault, Orb, Aude, Agly, Têt and Tech (Bourrin et al., 2006). For the past several years, monitoring has been implemented on different rivers, in particular the Têt River (Serrat et al., 2001) and the Rhône River in the western and the eastern part of the Gulf, respectively. These monitoring programmes have confirmed that most of the sediment fluxes from rivers occurred during flood events such as those recorded in 1994, 2002 and 2003 (Antonelli et al., 2008; Rolland, 2006; Miralles et al., 2006).

Sedimentary processes near river mouths have been the subject of many studies for the past several decades throughout the world, especially for the most important bodies such as the Mississippi River (Allison et al., 2005; [Corbett et al., 2004] and [Corbett et al., 2007]), the Amazon (Nittrouer and De Master, 1986; Nittrouer et al., 1995; Kuelh et al., 1995; Moore et al., 1995; Sternberg et al., 1996), the Eel River (Sommerfield and Nittrouer, 1999; Curran et al., 2002; Wheatcroft and Drake, 2003; Guerra et al., 2006 J.V. Guerra, A.S. Ogston and R.W. Sternberg, Winter variability of physical processes and sediment-transport events on the Eel River shelf, northern California, *Cont. Shelf Res.* 26 (2006), pp. 2050–2072. Article | PDF (1075 K) | View Record in Scopus | Cited By in Scopus (5)Guerra et al., 2006)

1  
2  
3  
4  
5  
6  
7  
8  
9  
10  
11  
12  
13  
14  
15  
16  
17  
18  
19  
20  
21  
22  
23  
24  
25  
26  
27  
28  
29  
30  
31  
32  
33  
34  
35  
36  
37  
38  
39  
40  
41  
42  
43  
44  
45  
46  
47  
48  
49  
50  
51  
52  
53  
54  
55  
56  
57  
58  
59  
60  
61  
62  
63  
64  
65

and the Po (Fox et al., 2004; Syvitski et al., 2005; Palinkas et al., 2005, 2007; Fain et al., 2007; Milligan et al., 2007). For the Gulf of Lions, these processes have been studied in the framework of the Eurostrataform programme, primarily in the Têt prodelta (Guillén et al., 2006; Law et al., 2008); whereas the Rhône system has not received the same attention until now.

The prodeltas of these rivers (Pauc, 2005) have been shown to be efficient traps for river-borne sediments and associated contaminants (Charmasson, 1998; Radakovitch et al., 1999; Charmasson, 2003; Roussiez et al., 2005). However, these areas can not be considered as final repositories because resuspension, remobilisation and displacement processes of sediments and particle-bound elements are expected, due to the effects of waves and currents (Lansard et al., 2006; Radakovitch et al., 2008). In these shallow waters, it is thus important to quantify the processes of sediment dynamics in relation to physical forcing linked to high energy events such as floods and storms (Bourrin et al., 2007).

A project (CARMA, french acronym for Consequences of Rhône River Inputs to the Associated Coastal Environnement) was thus implemented and this publication presents results obtained during the winter 2006-2007. The aims of this first event-response survey were: i) to characterise storm/discharge events and, ii) evaluate their relationship with sedimentation and erosion records in the Rhône prodelta area by means of different tools like radiotracers, iii) calculate the inventories of sediments and  $^{137}\text{Cs}$  on a part of the prodelta. The goal is also to follow the impact of extreme meteorological events on the prodelta sedimentary bed thanks to the installation of autonomous **instruments**, which had not been used until now in the study area.

### *1.1. The local setting*

With a catchment area of 95,500 km<sup>2</sup> and a mean flow-rate of 1700 m<sup>3</sup> s<sup>-1</sup>, the Rhône river is the main source of water and sediments in the western Mediterranean Sea. The river is 814 km long with its source in the Alps. As described by Arnaud-Fassetta et al. (2003), it crosses many different environnements and has varied during time with the different climatic periods. Its mouth opens

1 onto a prodelta that receives annual amounts of particles between 2 and 20 Mt (Sabatier et al.,  
2 2006; Eyrolle et al, 2006; Pont et al, 2002).

3 This subaqueous prodelta (30 km<sup>2</sup>) is composed of coarse grains comprising sands (> 63µm)  
4 forming sandy bars, and of fine grains constituted of clays (< 4µm) and silts (4 µm to 63 µm)  
5 (Aloisi and Monaco, 1975).  
6  
7

8  
9 The area chosen for instrument deployment in the framework of the CARMA project is very  
10 close to the Grand Rhône River mouth (Fig. 1), on the prodelta, at the boundary with the  
11 Camargues marshes on the west and the oil industry of Fos-sur-mer (Bouches-du-Rhône) on the  
12 east. Here the level of risk was considered acceptable for positioning permanent instrumentation.  
13  
14

15 The estuary is not considered to be influenced by Mediterranean Sea tides (microtidal), even if  
16 several centimetres high, but primarily by marine currents and swells. In addition, depending on  
17 their directions and intensities, superficial and bottom currents play different roles, e.g. suspension  
18 transport, erosion, deposition, etc. (Naudin et al., 1997; Maillet et al., 2006). Winds have  
19 considerable effects on hydrodynamics and sediment transport.  
20  
21  
22  
23  
24  
25  
26  
27  
28  
29  
30

### 31 32 33 34 *1.2. Flood events* 35 36

37 Because of its size, the Rhône valley is subject to different kinds of floods: mediterranean,  
38 oceanic, cevenol and generalised (Rolland, 2006). On December 4, 2003, an exceptional flood  
39 occurred with maximum river discharge reaching 11500 m<sup>3</sup> s<sup>-1</sup> in Arles. Because of the rapidity of  
40 the water rise (nearly 8000 m<sup>3</sup> s<sup>-1</sup> in 30 h, according to Antonelli et al. (2008), dykes burst and the  
41 banks broke, leading to large masses of solid suspended matter being carried over.  
42  
43  
44  
45  
46  
47  
48

49 Flood events are therefore important for the supply of material to the coastal area: it was estimated  
50 that the Rhône River releases 80% of the annual amount of sediments in several days of flooding  
51 (Rolland, 2006). At the same time, floods discharge tremendous amounts of radionuclides.  
52 Antonelli et al. (2008) calculated that  $77 \pm 16$  GBq of <sup>137</sup>Cs were released by the Rhône River  
53 during the exceptional flood (December 2003), although Rolland (2006) found an amount of 158  
54 GBq (48.7%) during the entire year 2003. Miralles et al. (2006) estimated that  $75 \pm 21$  GBq of  
55  
56  
57  
58  
59  
60  
61  
62  
63  
64  
65

1  
2  
3  
4  
5  
6  
7  
8  
9  
10  
11  
12  
13  
14  
15  
16  
17  
18  
19  
20  
21  
22  
23  
24  
25  
26  
27  
28  
29  
30  
31  
32  
33  
34  
35  
36  
37  
38  
39  
40  
41  
42  
43  
44  
45  
46  
47  
48  
49  
50  
51  
52  
53  
54  
55  
56  
57  
58  
59  
60  
61  
62  
63  
64  
65

$^{210}\text{Pb}$  in excess of its background ( $^{210}\text{Pb}_{\text{xs}}$ ) and  $27 \pm 2$  GBq of  $^{137}\text{Cs}$  were deposited during the flood of December 2003. Radioactive tracers can be used to follow sedimentary masses and enable to calculate sediment accumulation rates near the Rhône River mouth.

### 1.3. *Wind stress*

Two main types of winds affect the studied area. They are either originated from north, called Mistral, or from south-east, called Marin, and can be very strong during several days. The first one is channelized in the Rhône River valley and delivers cold air. The second one comes from offshore and is responsible of high waves generation.

## 2. **Material and methods**

The CARMA project started in September 2006 with the immersion of the first instruments in the Grand Rhône River mouth, near the Roustan Est buoy, and terminated by the CARMEX campaign in March 2007 (Fig. 1).

### 2.1. *Seabed and currents monitoring*

The results detailed here are from a S-ALTUS altimeter located near the Roustan Est buoy at a depth of 18 m. It was placed 64 cm above the bottom and recorded its distance to the floor every 15 minutes. The principle relies on the emission/reception of an acoustic beam by a cylindrical sensor during 30 ms with a frequency of 2 MHz (Jestin et al, 1998). The accuracy and resolution of the ALTUS were respectively 0.41 mm and 2 mm.

In addition, a RDI<sup>TM</sup> Workhorse Sentinel Acoustic Doppler Current Profilers (ADCP) was also immersed at 18 m depth right of the river mouth at the Roustan Est buoy. The transducers emitted 600 kHz beams and received an acoustic signal which frequency was different due to Doppler Effect.

1 Since the ADCP was set at 50 cmab, therefore the first available data was located 155 cmab. The  
2 ADCP yielded current data every 18 seconds and averaged them every 15 minutes along 40 depth  
3 cells 50 cm high, with an accuracy of  $0.51 \text{ cm s}^{-1}$ . Backscattering was measured by an electric  
4 signal as counts, transformed into an energy balance in decibels, linking the emission and  
5 reception levels of the acoustic wave. MATLAB was used to correct the attenuation effects of  
6 interfering parameters such as the water column (model of François and Garrison, 1982; Tessier,  
7 2006), near field correction factor (Downing formulation), propagation length and the air-water  
8 interface. These backscattering values in dB, however, are relative and cannot be compared to  
9 other backscattering data from other ADCPs. They qualitatively show backscattering variations,  
10 linked to turbidity, during this period. Unfortunately, not enough suspended sediment matter  
11 (SSM) concentrations were measured so as to calibrate the ADCP data precisely but a calibration  
12 has been estimated thanks to samples from the CARMEX campaign in March 2007 (Dufois,  
13 2008).

## 31 *2.2. Waves and winds modelling*

32  
33  
34  
35 The ALADIN atmospheric meso-scale model of Météo-France shows the wind conditions in the  
36 Grand Rhône River mouth area ( $43.3^\circ \text{ N}$ ,  $4.8^\circ \text{ E}$ ). Each node of the grid in this area is separated by  
37 3 km. This weather profile covered the entire study period, showing the wind intensity and  
38 direction. Wave fields were modelled in the western Mediterranean Sea with a resolution of  $0.1^\circ$   
39 using the third generation WAVEWATCH-III wind-wave model (Tolman, 2002a) forced by  
40 Météo-France wind fields. This model, developed at NOAA/NCEP and adapted from the WAM  
41 model, has been successfully applied in global- and regional-scale studies in many areas  
42 throughout the world's oceans (Chu et al., 2004), in particular in the western Mediterranean Sea  
43 (Ardhuin et al., 2007). The model is based on the two-dimensional wave action balance equation  
44 including energy density generation and dissipation terms by wind, white-capping, wave-bottom  
45 interaction, and redistribution of wave energy due to wave-wave interactions. The model was  
46  
47  
48  
49  
50  
51  
52  
53  
54  
55  
56  
57  
58  
59  
60  
61  
62  
63  
64  
65

validated and compared to other models for two periods in 2002 and 2003 (Ardhuin et al., 2007) and in 2001 (Dufois, 2008).

The current-induced bottom shear stress BSS ( $\tau_c$ ) was calculated with the assumption that the velocity profile is logarithmic down to the first layer of the ADCP above the bottom:

$$\tau_c = \rho u_{*c}^2 \text{ with } u_{*c} = \frac{\kappa u(z)}{\ln(z/z_0)} \quad (1)$$

where  $\rho$  is water density,  $\kappa$  the Von Karman constant ( $=0.4$ ),  $z$  the height of the first layer above the bottom,  $u(z)$  the associated velocity and  $z_0$  the bed roughness. Since the sediment is cohesive in this area,  $z_0$  was set at 0.1 mm, a typical value found in the literature (Soulsby, 1997).

For the wave-induced BSS ( $\tau_w$ ) we used the usual formulation, which depends on orbital velocity  $U_b$  just above the bed:

$$\tau_w = 0.5 \rho f_w U_b^2 \quad (2)$$

with (Swart, 1974)  $f_w=0.3$  if  $A/k_s < 1.57$ ,

$$\text{and beyond: } f_w = 0.00251 \exp(5.21(A/k_s)^{-0.19}), \quad (3)$$

where  $A$  is the orbital half-excursion near the bottom ( $A = \frac{U_b T}{2\pi}$ ,  $T$  being the wave period).

The total BSS was calculated by direct addition of wave-induced BSS and the current-induced BSS without taking non-linear wave-current interactions into account.

### *2.3. Radionuclide geochronology and particle size: sampling and analyses*

Four of the nine sediment cores sampled during the CARMEX cruise (March 11-17, 2007, RV L'Europe) were analysed for their grain size distribution and/or to estimate sediment accumulation rates in this area. US04Kb was sampled close to the instruments location, USCh30 and USCh20 in channel-like structures, while USHCh20 was located nearby but out of **these bottom structures**. They were sub-sampled twice using circular Plexiglas tubes (18 cm diameter, 50 cm long) in box-cores collected by USNEL (large volume box-corer) carefully maintaining the sediment-water interface undisturbed. The length of the cores varied from 34 to 40 cm and their sampling depths

1 were 22 to 49 m on the continental shelf. These cores were sliced in 1 cm sections. Each 1 cm  
2 thick sediment layer was dried, crushed, passed through a 200  $\mu\text{m}$  sieve and put in 200 mL and 60  
3 mL geometries for gamma spectrometry investigations. These analyses were conducted at the  
4 IRSN laboratory in Orsay, near Paris, with N-type hyper-purity germanium detectors in 200 mL  
5 volume containers and measured with a counting time of 20 or 40 h. Efficiency calibrations from  
6 22.5 keV to 1.8 keV were carried out using mixed gamma-ray sources in a solid resin-water  
7 equivalent matrix with a density of 1.15  $\text{g cm}^{-3}$  (Bouisset et Calmet, 1997). Activity results were  
8 corrected for true coincidence summing and self-absorption effects.  $^7\text{Be}$ ,  $^{137}\text{Cs}$ ,  $^{210}\text{Pb}$  and  $^{234}\text{Th}$   
9 were determined.

10  $^7\text{Be}$  ( $t_{1/2}=53.2$  d) is a natural radionuclide, resulting from the cosmic ray spallation of nitrogen and  
11 carbon in the atmosphere. It was analysed in order to determine particulate deposit up to 200 days  
12 and even more. It settles on the river-bed, bounds to detritic particles and spreads in marine  
13 systems via river discharges (Canuel et al., 1990). Palinkas et al. (2005) suggested to perform  
14 several sedimentological analyses to confirm the short-time-scale sediment accumulation rates  
15 found with  $^7\text{Be}$ .

16  $^{137}\text{Cs}$  ( $t_{1/2}=30.1$  y) is an anthropogenic radionuclide and originated from nuclear tests, nuclear  
17 accidents such as Chernobyl in April 1986, and nuclear power plant discharges, i.e. the spent fuel  
18 reprocessing site at Marcoule. It has a high affinity for clays and fine particles in fresh water and  
19 has been found to be a good tracer of the Rhône River inputs to the Gulf of Lions.  $^{137}\text{Cs}$  depth  
20 profiles **have been extensively used** in various environments to assess sediment accumulation rates,  
21 notably coupled with  $^{210}\text{Pb}_{\text{xs}}$  (Appleby et al., 1979; Nittrouer et al., 1983/1984; He and Walling,  
22 1995; Radakovitch et al., 1999; Frignani et al., 2004).

23  $^{210}\text{Pb}$  ( $t_{1/2}=22.3$  y) is a naturally occurring radionuclide produced in soil, sediment and water by the  
24 decay in the atmosphere of  $^{226}\text{Ra}$  through its daughter  $^{222}\text{Rn}$ . The cycle ends in lacustrine and  
25 marine sediments where two types of  $^{210}\text{Pb}$  can be found: that produced in situ (called supported)  
26 and that coming with the accumulated particles (called unsupported or excess). Because of its



specific half-life, excess  $^{210}\text{Pb}$  ( $^{210}\text{Pb}_{\text{xs}}$ ), calculated by removing  $^{214}\text{Pb}$  to total  $^{210}\text{Pb}$ , is useful for assessing centennial sediment accumulation rates in marine systems (Miralles et al., 2005).

$^{234}\text{Th}$  ( $t_{1/2}=24.1$  d) is a radiogenically produced radionuclide, arising from the decay of  $^{238}\text{U}$  dissolved in seawaters. Due to its high affinity for particles, it is soon delivered to sediments and its short half-life enables particulate dynamics and sedimentation to be assessed during flood events. Also in this case, the dating parameter is in excess ( $^{234}\text{Th}_{\text{xs}}$ ) over the fraction produced in situ.

Radionuclide activities were corrected for the decay over the time elapsed between sampling and counting. Furthermore,  $^{137}\text{Cs}$  depth profiles do not show any dating feature because of the length of the sediment cores, the low activities and the absence of the end of the signal.

An aliquot of fresh sediment from each layer was kept for grain-size characterisation, using a Beckmann & Coulter LS 13320 laser grain sizer, with multi-wavelength technology called Polarization Intensity Differential Scattering (PIDS) enabling a better accuracy for clay fractions. Fresh sediments were placed in 5 cL plastic tubes and diluted with water to obtain a concentration close to  $10 \text{ g L}^{-1}$ . Ten mL of these solutions were analysed with the laser grain sizer. Three replicates were analysed for each sample and were averaged to verify the quality of the results. The range of analysis was  $0.4 \mu\text{m}$  to  $2000 \mu\text{m}$  with an accuracy of 3% for median size and 5% for each side of the distribution profile. Five ranges have been used to classify the grain sizes: clays ( $<4 \mu\text{m}$ ), fine silts (4 to  $20 \mu\text{m}$ ), coarse silts (20 to  $63 \mu\text{m}$ ), fine sands (63 to  $200 \mu\text{m}$ ) and coarse sands ( $>200 \mu\text{m}$ ). Values of D10, D50 and D90 were calculated, representing respectively the maximum diameter of 10%, 50% and 90% of the sediment samples.

Inventories were obtained thanks to ArcGIS® and Surfer® softwares, processing data from the sediment cores sampled during CARMEX with interpolation methods.

### 3. Results

#### 3.1. Rhône River flow rate

1  
2  
3  
4  
5  
6  
7  
8  
9  
10  
11  
12  
13  
14  
15  
16  
17  
18  
19  
20  
21  
22  
23  
24  
25  
26  
27  
28  
29  
30  
31  
32  
33  
34  
35  
36  
37  
38  
39  
40  
41  
42  
43  
44  
45  
46  
47  
48  
49  
50  
51  
52  
53  
54  
55  
56  
57  
58  
59  
60  
61  
62  
63  
64  
65

Fig. 2a and Fig. 2b show water flows of the Rhone River (at the Beaucaire station, just upstream from the separation between the Grand Rhône River and the Petit Rhône River) and of its upstream tributaries (Isère, Gard, Ardèche, Saône, Perrache, Cèze, Ouvèze). Flood threshold ( $3000 \text{ m}^3 \text{ s}^{-1}$ ) was exceeded in Beaucaire on November 18, 2006 ( $3775 \text{ m}^3 \text{ s}^{-1}$ ) and on December 9, 2006 ( $3520 \text{ m}^3 \text{ s}^{-1}$ ). These flows are likely to provide enough sediment to significantly impact the prodelta and to the Gulf of Lions.

The increased flow rate in Beaucaire and at the Rhône river mouth on November 18, 2006 resulted from an increase in the flow-rates of the Cèze, Gard and Ardèche rivers (Fig. 2b), which are Cevenol rivers, reaching values three times their flood discharge thresholds and with a return period lower than 2 years. The origin of this high Rhône river flow was undoubtedly a Cevenol flash flood (Maréchal, 2006; Antonelli et al., 2008). On the contrary, the flood of December 9 is of oceanic type. In this case, the entire catchment area undergoes an increase of water flow: upstream rivers multiply their mean flows by a factor of 6 and downstream rivers from 3- to 5- fold (Fig. 2a).

### 3.2. *Wind conditions*

Several episodes of violent and cold northerly winds (the Mistral) occurred during the study period, with velocities reaching  $20 \text{ m s}^{-1}$ . This Mistral was in fact the strongest wind ever recorded here and the most frequent between November 8, 2006 and February 22, 2007. Some southeast winds blew in from the sea, creating turbulence on surface waters. They reached  $20 \text{ m s}^{-1}$  and considerably increased turbidity (Fig. 3b and Fig. 3e), combined with high river flow. These winds create a swell when they are continuously active during a quite long time (Fig. 3e and Fig. 3g) whereas long periods of Mistral winds do not cause considerable swells. In fact, winds from the north (between  $300^\circ\text{N}$  and  $50^\circ\text{N}$ ) cause no or only weak swells, with heights less than one metre. Southerly and easterly winds from the Mediterranean Sea, however, caused an increase in swell formation, especially from mid-November to mid-December 2006 and on February 18, 2007 when a swell peak reached a height of 3 m.

### 3.3. Data recorded in situ

1 Fig. 3 (a,b,c) shows current velocities and directions recorded near the Roustan Est buoy and the  
2 backscattered signal in the water column from November 8, 2006 to February 22, 2007. Superficial  
3 currents were primarily in the southwest direction until December 13, 2006. When the wind  
4 changed direction (Fig. 3e), i.e. a southeast wind was replaced by a north wind (Mistral); currents  
5 then changed direction, toward the southeast. In any case, no clear stratification appeared on  
6 profiles, since orientation was practically unchanged in the entire water column. On the contrary,  
7 velocity decreased with depth. The primary reason is that the currents induced were caused by  
8 winds, not by density variations.  
9

10 On November 18, 2006, current velocities (Fig. 3b), reached  $50 \text{ cm s}^{-1}$  and did not change very  
11 much with depth ( $30 \text{ cm s}^{-1}$ , 1.5 mab). At the same time, the ADCP recorded a backscattered signal  
12 of 90 dB. Higher values of backscattering were recorded (100 dB) on November 20, 2006, related  
13 to a southeast (SE) wind velocity of  $8 \text{ m s}^{-1}$ . The period of SE winds was characterised by swell  
14 waves, causing bottom shear stress. Swell heights peaked (Fig. 6g) on November 20 (1.8 m),  
15 December 9, 2006 (1.9 m), January 24 (2 m) and February 18, 2007 (2.9 m) increasing the  
16 backscattering signal (80 to 100 dB).  
17

18 The second flood period (December 9, 2006) occurred while Mistral winds were blowing at a  
19 velocity of  $15 \text{ m s}^{-1}$ , despite a short episode of SE winds. In general, northerly winds are more  
20 intense than southeast winds but they need to last in time to induce bottom shear stress. The  
21 backscattered signal high level lasted for 4 days, corresponding to the increased flow-rate.  
22 Suspended matter was well concentrated but had a low velocity: 95 dB with  $3$  and  $30 \text{ cm s}^{-1}$  at 1.5  
23 mab and at the surface, respectively. The intense acceleration of superficial currents between  
24 November 23 and 29, 2006, shows the role of SE winds that influenced the surficial layer, down to  
25 more than 5 m beneath the water surface, for 5 days. They caused an important swelling (Fig. 3g)  
26 and resulted in the settling of suspended particles and the resuspension of bottom sediment, as  
27 shown in Fig. 3c.  
28  
29  
30  
31  
32  
33  
34  
35  
36  
37  
38  
39  
40  
41  
42  
43  
44  
45  
46  
47  
48  
49  
50  
51  
52  
53  
54  
55  
56  
57  
58  
59  
60  
61  
62  
63  
64  
65

1 On January 24, 2007, the peak in swell height (2 m) was concomitant with an increase in Rhône  
2 River flow ( $2200 \text{ m}^3 \text{ s}^{-1}$ ) leading to an acceleration of the surface currents (nearly  $80 \text{ cm s}^{-1}$ ).  
3 Similarly, on February 18, 2007 the series of highest waves of the study was recorded (2.9 m)  
4 during strong SE winds ( $20 \text{ m s}^{-1}$ ) together with an increase in flow-rate ( $2500 \text{ m}^3 \text{ s}^{-1}$ ) leading to  
5 relatively constant southwest current velocity ( $> 60 \text{ cm s}^{-1}$ ) in the water column (Fig. 4).  
6  
7  
8  
9

### 10 11 3.4. *Sediment characteristics* 12

13  
14  
15 Core US04Kb, taken from a site close to the position of the instruments (Fig. 1), shows a mean  
16 grain diameter of  $15.3 \text{ }\mu\text{m}$ , i.e. the size of fine silts, when averaging the topmost 5 cm (Fig. 7). The  
17 core was composed of 15 % of clays, 70 % of silts and 15 % of sands. These values are  
18 characteristics of the entire prodelta area (Radakovitch et al, 1999; Miralles et al., 2006).  
19

20 Fig. 3d shows the distance between the altimeter transducer and the prodelta bottom during the  
21 study period. The net balance in deposition/erosion processes between November 2006 and  
22 February 2007 is almost zero. Nevertheless, important changes occurred on a shorter time scale.  
23 These changes appear to be linked to changes in environmental conditions recorded in parallel. It  
24 is to be stressed that several „blank’ periods in Fig. 3d, were due to very high SSM concentrations  
25 or something that temporarily interfered with the transducer beam.  
26  
27  
28  
29  
30  
31

32 The quantitative understanding of these records requires calculation of the BSS occurred during  
33 our experiment and link their values to sediment suspension and erosion (Fig. 5).  
34

35 Series of waves, combined with currents, created a succession of BSS between  $1.5$  and  $2 \text{ N m}^{-2}$   
36 and, as a consequence, Bottom Backscattering Indices (BBI), related to suspended solid  
37 concentrations, were close to 70 to 80 dB. The greatest BBI, approaching 100 dB, occurred during  
38 strong water flows (more than mean liquid discharge) but considerable BSS also increased BBI.  
39  
40  
41  
42  
43

44 Two periods of accretion appeared on the altimetric profile of Fig. 3d, exactly during or just after  
45 the high Rhône River discharges. The first deposition time D1 occurred on November 18 and  
46 increased the bottom level by 5 cm in less than 3 days: the distance between the transducer and the  
47 floor (DTF) decreased from 63.5 cm to 58.5 cm. The second deposition time D2 occurred on  
48  
49  
50  
51  
52  
53

1  
2  
3  
4  
5  
6  
7  
8  
9  
10  
11  
12  
13  
14  
15  
16  
17  
18  
19  
20  
21  
22  
23  
24  
25  
26  
27  
28  
29  
30  
31  
32  
33  
34  
35  
36  
37  
38  
39  
40  
41  
42  
43  
44  
45  
46  
47  
48  
49  
50  
51  
52  
53  
54  
55  
56  
57  
58  
59  
60  
61  
62  
63  
64  
65

November 9, 2006, and reduced the DTF by 6 cm (62 cm to 56 cm) in 9 days. The D1 event corresponded to a flow increase of nearly  $3000 \text{ m}^3 \text{ s}^{-1}$  in 36 h and a flood duration of 24 h, while the D2 event corresponded to a flow increase of  $2300 \text{ m}^3 \text{ s}^{-1}$  in 6 days and a flood duration of 3 days. Between these two deposition phases, an erosion phase E1 removed at least 4.5 cm of sediment, probably due to a succession of high BSS values (Fig. 5).

On February 18, 2007, almost 4 cm of sediment disappeared in only several hours during an erosive event E2. At this time, both  $15 \text{ m s}^{-1}$  SE winds with 3 m high waves and Rhône river flow around  $2500 \text{ m}^3 \text{ s}^{-1}$  induced  $60 \text{ cm s}^{-1}$  bottom currents oriented southeast and a BSS of  $5 \text{ N m}^{-2}$ . The latter was due primarily to waves (90%) and led to peak values reaching 93 dB in BBI (Fig. 5a).

No special event was recorded during the second half of December, a month characterised primarily by compaction processes and early diagenesis.

A thin deposition on January 3, 2007, confirmed by BBI of 90 dB, appeared just after an increase in water flow of  $1300 \text{ m}^3 \text{ s}^{-1}$ .

On January 24, 2007, inputs from the Rhône River (flows higher than  $2000 \text{ m}^3 \text{ s}^{-1}$ ) and the strong influence of waves (BSS of  $2.6 \text{ N m}^{-2}$ ) caused increases of the backscattered signal in the water column (Fig. 3c) and the bottom layer (Fig. 5a), with no intense accretion or erosion recorded (Fig. 3d). Except for these two January events, the mid-December to mid-February period characterised by both low river discharges and wave effects, the water-sediment interface remained regular and almost flat.

Cores sampled during the oceanographic campaign, i.e. almost 17 days after the last data recorded in situ (Fig. 6), showed that fine fractions (clays and silts) were prevailing but more sands were recently deposited (Fig. 7).

Station US04Kb was **the closest to the mooring**, at a distance of 100 m and a depth of 25 m. Layers 3 cm thick with 10% coarse sand appeared at the water-sediment interface, whereas the sandy component downcore (ca. 10%) was finer. This shows a recent, substantial and sudden input.

1  
2  
3  
4  
5  
6  
7  
8  
9  
10  
11  
12  
13  
14  
15  
16  
17  
18  
19  
20  
21  
22  
23  
24  
25  
26  
27  
28  
29  
30  
31  
32  
33  
34  
35  
36  
37  
38  
39  
40  
41  
42  
43  
44  
45  
46  
47  
48  
49  
50  
51  
52  
53  
54  
55  
56  
57  
58  
59  
60  
61  
62  
63  
64  
65

CNR (french acronym of National Company of the Rhône River) data, obtained from continuously recording of sediment hydrodynamic times, showed a flood event just before the core sampling time (Fig. 6). Altimeter data proved that Rhône river discharges more than  $3000 \text{ m}^3 \text{ s}^{-1}$ , even with wave effects, caused deposit of sediments. The fraction of coarse grains was probably due to this increase of river flow, since absolute bottom depth remained constant from November 8, 2006, to February 22, 2007. This third flood event reached an average flow peak of  $3667.2 \text{ m}^3 \text{ s}^{-1}$  and remained above the  $3000 \text{ m}^3 \text{ s}^{-1}$  threshold for one week. It seems to have been the origin of the deposit of 3 to 5 cm of sandy sediments close to the Rhône river mouth. The fact that three high flow events succeeded each other and that they were synchronous with successions of high waves, did not enable the sandy layers to deposit for a long time and be covered by fine grain sediments. There is thus no very definite peak of coarse sands in the different cores but some thin layers appear.

### 3.5. *Sediments accumulation*

Apparent sediment accumulation rates were roughly calculated in three cores collected just in front of the Rhône River mouth (USChenal20m, USChenal30m and USHChenal20m) using radiotracer activity depth distributions (Fig. 8).  $^{137}\text{Cs}$  and  $^{210}\text{Pb}_{\text{xs}}$  profiles are strongly correlated. However, due to the end of reprocessing operations in Marcoule,  $^{137}\text{Cs}$  activities are quite low compared to the values observed before 1997 (Charmasson, 1998).  $^{137}\text{Cs}$  values ranged from  $3.1 \text{ Bq kg}^{-1}$  to  $16.5 \text{ Bq kg}^{-1}$  in the three cores. Their  $^{137}\text{Cs}$  inventories were  $8900 \text{ Bq.m}^{-2}$ ,  $7604 \text{ Bq.m}^{-2}$  and  $8470 \text{ Bq.m}^{-2}$ , respectively.

Total radioactivities of  $^{210}\text{Pb}$  (also for  $^{210}\text{Pb}_{\text{xs}}$ ) varied according the same change of  $^{137}\text{Cs}$ : signal increases and decreases occurred at the same depth. Concentrations ranged from  $31.2$  to  $118 \text{ Bq kg}^{-1}$  in the three cores. Their  $^{210}\text{Pb}_{\text{xs}}$  inventories were  $53647 \text{ Bq.m}^{-2}$ ,  $67604 \text{ Bq.m}^{-2}$  and  $61347 \text{ Bq.m}^{-2}$ , respectively. USC20 and USC30 are two channel-like stations which apparently accumulated more radionuclides than USHC20, as shown by comparing the activity ranges. This

can result from the fact that channel-like structures are preferential pathways for sediments for all the size scales (canyons, channels).

Strong dilution signatures are not really visible on  $^{137}\text{Cs}$  and  $^{210}\text{Pb}_{\text{xs}}$  profiles, in comparison with studies realised by Miralles et al. (2006) and Drexler et Nittrouer (2008) on Rhône River floods. However, their flow rates were more important compared to our case.

The depth profiles of  $^{137}\text{Cs}$  and  $^{210}\text{Pb}$  are not suitable to calculate sediment accumulation rates. None of the classical models for  $^{210}\text{Pb}$  dating can be applied to this very dynamic environment, due to episodic and inconstant delivery. However,  $^7\text{Be}$  and  $^{234}\text{Th}_{\text{xs}}$  patterns permitted to estimate recent sediment deliveries, by dividing the depth of the base of the profiles by 5 times the half lives of the radionuclides.

The  $^7\text{Be}$  signal ceases at 16, 14 and 10 cm depth in cores USC20, USC30 and USHC20, respectively. The base of the  $^7\text{Be}$  depth profile reflects the beginning of the accumulation of fresh sediment, i.e. almost 200 days. USHC20 accumulated less sediment than the other cores, as explained above. Integrated over the entire year, the calculated maximum sediment accumulation rates are  $29.2 \text{ cm y}^{-1}$ ,  $46.6 \text{ cm y}^{-1}$  and  $53.3 \text{ cm y}^{-1}$  for USHC20, USC30 and USC20, respectively.

$^{234}\text{Th}_{\text{xs}}$  signals disappear between 3 and 3.5 cm in each core but there were abrupt peaks at 5, 8 and 11 cm with intensities of 51.7, 152.4 and 154.5  $\text{Bq kg}^{-1}$ , for USHC20, USC30 and USC20, respectively. These results would confirm that apparent sediment accumulation rate at USC20 is slightly higher than at USC30 and much higher than at USHC20. Signals completely disappeared at depths of 5.5, 11.5 and 13 cm, respectively. The first three centimetres were probably deposited very recently, during the last flood (from March 3 to 10, 2007), as it is showed by the core US04Kb. Nevertheless, the peaks would reflect that previous inputs of sediments occurred in December and/or November 2006 (Fig. 8). In this case, maximum sediment accumulation rates were estimated between 16.5 and 22  $\text{cm y}^{-1}$  for USHC20, between 34.5 and 46  $\text{cm y}^{-1}$  for USC30 and between 39 and 52  $\text{cm y}^{-1}$  for USC20. The sediment accumulation rates calculated using  $^7\text{Be}$  and  $^{234}\text{Th}_{\text{xs}}$  are thus quite similar.

1  
2  
3  
4  
5  
6  
7  
8  
9  
10  
11  
12  
13  
14  
15  
16  
17  
18  
19  
20  
21  
22  
23  
24  
25  
26  
27  
28  
29  
30  
31  
32  
33  
34  
35  
36  
37  
38  
39  
40  
41  
42  
43  
44  
45  
46  
47  
48  
49  
50  
51  
52  
53  
54  
55  
56  
57  
58  
59  
60  
61  
62  
63  
64  
65

The decrease of hydrodynamics is evident in USHC20 at the depth of 11 cm, with a sandy fraction diminishing from more than 20% to less than 3% (along a 5 cm layer), and with D50 and D90 from 6  $\mu\text{m}$  to 20  $\mu\text{m}$  and from 20  $\mu\text{m}$  to 120  $\mu\text{m}$ , respectively (Fig. 7). A decrease in accumulation rate with consequent increase of  $^{210}\text{Pb}_{\text{xs}}$  activity is visible (Fig. 8). USHC20 revealed a 17 cm homogeneous layer (13.4  $\text{Bq kg}^{-1}$  and 99.5  $\text{Bq kg}^{-1}$  for  $^{137}\text{Cs}$  and  $^{210}\text{Pb}_{\text{xs}}$ ), followed by a decrease (3.6  $\text{Bq kg}^{-1}$  and 34.6  $\text{Bq kg}^{-1}$ ) and then an increase (12.6  $\text{Bq kg}^{-1}$  and 69  $\text{Bq kg}^{-1}$ ) at 29 cm beneath the sediment surface for both  $^{137}\text{Cs}$  and  $^{210}\text{Pb}_{\text{xs}}$ . USC20 and USC30 also show this pattern, even if it is not as well-defined as USHC20. Grain size and radiotracers concentrations signals are really concomitant and account for the April 2006 Rhône River flood (4164  $\text{m}^3 \text{s}^{-1}$ ). Drexler et Nittrouer (2008) normalised the excess  $^{210}\text{Pb}$  with the clay content to remove the effects related strictly to grain size. They observed a dilution signature in their  $^{210}\text{Pb}_{\text{xs}}$  profiles, accounting for an increase of the high river flow.

The end of the  $^7\text{Be}$  signal corresponds to almost 200 days and to 100 days for  $^{234}\text{Th}_{\text{xs}}$  (Palinkas et al., 2005) and did not cease at the same depths. This would mean that the winter events (last 100 days) caused heterogeneous accumulation rates, although during the preceding 100 days, the ASR was constant according to 3 cores (from 3 to 4.5 cm). This can be explained by the fact that hydrology and meteorology parameters are totally different in summer/autumn and in winter/spring.

#### 4. Discussion

The results presented here show a very good correlation between all the parameters studied: currents, waves and wind directions and intensities, backscattered signals, river discharges and sedimentary phases, BSS and BBI. Deposition phases in fact occurred during the two flood events, erosion episodes occurred while waves effects were greatest and southeast winds were correlated with swell impacts and high BBI.



#### 4.1. Impact of storms

1 Bourrin et al. (2007) monitored the Têt prodelta during wet and dry storms, i.e. during strong  
2 wave events associated with high and low river flows. Accretion phases were observed during wet  
3 storms, while dry storms led to erosion phases. Mean discharges of the Têt and the Rhône rivers  
4 are different,  $10 \text{ m}^3 \text{ s}^{-1}$  and  $1700 \text{ m}^3 \text{ s}^{-1}$ , but **sedimentary mechanisms occurring off their** mouths  
5 are similar. The critical shear stresses causing erosion evaluated in the laboratory for the Têt and  
6 the Rhône coastal areas are different:  $0.12 \text{ N m}^{-2}$  (Guillén et al., 2006; Bourrin et al., 2007) and  
7 from  $0.068$  to  $0.087 \text{ N m}^{-2}$  (Lansard et al., 2006), respectively. These latter data would correspond  
8 to the suspension of the fluffy layer.  
9

10 Recent experiments on the Rhône prodelta evaluated critical BSS of  $0.35 \text{ N m}^{-2}$  (Dufois, 2008).  
11 BSS exceeded  $1 \text{ N m}^{-2}$  six times in three months of relatively quiet periods on the Rhône prodelta,  
12 but only twice on the Têt prodelta during the intense storms that occurred in December 2003 and in  
13 January 2004. Bottom currents were directed south and southwest in both river mouths during  
14 these events.  
15

16 Altimetric records **showed** alternately deposition/erosion phases (from days to weeks) and the  
17 balance over the studied period is zero. The Bottom Boundary Layer (BBL), responsible for  
18 sediment dispersion over the Gulf of Lions (Monaco et al., 1999; Lansard et al., 2006), is fed by  
19 sediments resuspension processes, forming the Benthic Nepheloid Layer (BNL).  
20

21 Law et al. (2008) asserted that individual grain size classes of the BNL are being eroded in  
22 proportions equal to the seabed and verified the sorting of bottom sediment size distributions  
23 across the Têt River mouth. Sandy fractions and mean grain sizes decrease in the seaward direction  
24 and with increasing depth. The results are comparable to the Rhône River mouth in USC20 (22 m)  
25 and USC30 (49 m): from 19.2% to 1.8% sands and D50 from  $18.7 \mu\text{m}$  to  $13.6 \mu\text{m}$  (Fig. 7).  
26  
27  
28  
29  
30  
31  
32  
33  
34  
35  
36  
37  
38  
39  
40  
41  
42  
43  
44  
45  
46  
47  
48  
49  
50  
51  
52  
53  
54  
55  
56  
57  
58  
59  
60  
61  
62  
63  
64  
65

## 4.2. Hydrodynamics

Lansard (2005) deployed an ADCP near the Rhône River mouth from April 29 to June 5, 2002. The instruments did not record any flood but river flow and waves reached  $2700 \text{ m}^3 \text{ s}^{-1}$  (May 5) and 1.8 m high (May 8). During peak flow, the ADCP recorded **strong backscattered signals, the direction** of bottom currents was southwest during 55% of the study period and velocities were higher than  $15 \text{ cm s}^{-1}$  86% of the time. These observations are consistent with the conditions of the winter of 2006-2007.

The highest waves observed by Lansard (2005) were caused by southeast winds ( $90^\circ$  to  $180^\circ$ ) and led to BSS of  $0.4 \text{ N m}^{-2}$ . This value was exceeded by the highest 11 BSS results recorded during CARMA (with 5 events between  $1 \text{ N m}^{-2}$  and  $4.5 \text{ N m}^{-2}$ ). In agreement with the observations by Lansard (2005), each BSS peak was accompanied by high BBI, showing the resuspension of sediments after that critical erosion stress  $\tau_{\text{erosion}}$  was reached (established in a laboratory thanks to flume experiments in a channel). The minimum and maximum  $\tau_{\text{erosion}}$  were estimated as  $0.08 \text{ N m}^{-2}$  and  $0.12 \text{ N m}^{-2}$  at the Roustan Est buoy. The current-induced BSS exceeded the maximum  $\tau_{\text{erosion}}$  ( $0.35 \text{ N m}^{-2}$ ) by three-fold and reached  $0.55 \text{ N m}^{-2}$  during the storm of January 24, 2007.

In addition, two wave series were higher than 1.5 m in May 2002 compared to 8 wave series in the winter of 2006-2007, representing 10% of the study period. Winter periods with high flood events and strong storms (especially due to southeast winds), caused harsher environmental conditions for the Rhône River than in spring.

## 4.3. Apparent sediment accumulation rates (ASR)

The results are in agreement with Charmasson et al. (1998), who used  $^{137}\text{Cs}/^{134}\text{Cs}$  activity ratios to estimate sediment accumulation rates in the prodelta that ranged from 37 to  $48 \text{ cm y}^{-1}$  at the mouth by means of a several years study, and with Calmet and Fernandez (1990) with values of 30-35  $\text{cm y}^{-1}$ . Here,  $^{134}\text{Cs}$  is no more detectible preventing us from using  $^{137}\text{Cs}/^{134}\text{Cs}$  ratio to calculate sedimentation rates (Charmasson et al., 1998; Radakovitch et al., 1999). The range

1  
2  
3  
4  
5  
6  
7  
8  
9  
10  
11  
12  
13  
14  
15  
16  
17  
18  
19  
20  
21  
22  
23  
24  
25  
26  
27  
28  
29  
30  
31  
32  
33  
34  
35  
36  
37  
38  
39  
40  
41  
42  
43  
44  
45  
46  
47  
48  
49  
50  
51  
52  
53  
54  
55  
56  
57  
58  
59  
60  
61  
62  
63  
64  
65

evaluated is broad (from 29.2 to 53.3 cm y<sup>-1</sup> with <sup>7</sup>Be and from 16.5 to 52 cm y<sup>-1</sup> with <sup>234</sup>Th<sub>xs</sub>) because radionuclide concentrations were influenced by grain-size distributions. Radakovitch et al. (1999) obtained values higher than 20 cm y<sup>-1</sup> in the prodelta and 0.2 cm y<sup>-1</sup> over the shelf using the <sup>210</sup>Pb<sub>xs</sub> dating method and <sup>137</sup>Cs/<sup>134</sup>Cs activity ratios, confirmed by Zuo et al. (1996). Miralles et al. (2005) emphasised the difference between deposition in the Rhône River mouth (30-40 cm y<sup>-1</sup>) and the rest of the prodelta (0.65 cm y<sup>-1</sup>). Sedimentation rates strongly decrease with the **distance from the river** mouth.

According to published data, river mouths exhibit different ASRs: the Eel River with 0.4 cm y<sup>-1</sup> (Sommerfield et al., 1999) or 0.1 to 1 cm y<sup>-1</sup> (Wheatcroft and Drake, 2003), the Po River with 0.23 cm y<sup>-1</sup> (Palinkas et al., 2007) or 0.77 cm y<sup>-1</sup> (Frignani et al., 2005), the Amazon River with 10 to 60 cm y<sup>-1</sup> (Kuelh et al., 1995; Nitrouer et al., 1995), the Mississippi River with 2 cm y<sup>-1</sup> (Corbett et al., 2004) . Sediment accumulation rates are difficult to determine because physical (erosion, compaction, advection) and biogeochemical (bioturbation, early diagenesis, diffusion) processes interfere with radionuclide signals (Wheatcroft and Drake, 2003), and above all because of the high solid discharge variations at the river mouth.

#### 4.4. Fate of Rhône River inputs during the winter 2006-2007

During the two moderate floods periods, suspended sediments were carried southwest and south (Fig. 4) in the entire water column, with velocities decreasing with the depth. The coarsest particles deposited first near the mouth, feeding the sandy bar originated by the actions of the river and the waves. According to Thill (2001), during a low river discharge period (500 m<sup>3</sup> s<sup>-1</sup>), a saltwedge appears up to 20 km inland and is pushed seaward during a high river period (>2500 m<sup>3</sup> s<sup>-1</sup>). When fresh waters mix with salt waters, i) a portion of fine suspended sediment flocculates and settles to form larger entities contributing to the BNL (Curran et al., 2007) and ii) the remaining fraction moves seaward to form the Surface Nepheloid Layer (SNL) (Milligan et al., 2007). Other parameters/processes play a role in flocculation/deflocculation processes, such as organic matter contents, suspended sediment concentrations and particles-particles interactions.

1  
2  
3  
4  
5  
6  
7  
8  
9  
10  
11  
12  
13  
14  
15  
16  
17  
18  
19  
20  
21  
22  
23  
24  
25  
26  
27  
28  
29  
30  
31  
32  
33  
34  
35  
36  
37  
38  
39  
40  
41  
42  
43  
44  
45  
46  
47  
48  
49  
50  
51  
52  
53  
54  
55  
56  
57  
58  
59  
60  
61  
62  
63  
64  
65

Just before the first flood, Rhône River flow was between  $501 \text{ m}^3 \text{ s}^{-1}$  and  $560 \text{ m}^3 \text{ s}^{-1}$  for 2 days, causing the occurrence of a saltwedge and probably the flocculation of suspended particles. The 10 days following the first flood peak directed the SNL plume southwest with velocities reaching  $1 \text{ m s}^{-1}$ , although BSS resulting from waves and currents caused little suspension of BNL sediments ( $1 \text{ N m}^{-2}$ ). One day of weak northeast bottom circulation ( $15 \text{ cm s}^{-1}$ ) occurred during a long period of bottom southwest current velocities ranging from  $20 \text{ cm s}^{-1}$  to  $50 \text{ cm s}^{-1}$ . After this, both a wave-induced BSS of  $1.2 \text{ N m}^{-2}$  and the absence of river inputs enabled the erosion of the interface sediments, visible on the altimetric profile (November 26, 2006). While undergoing suspension, sediments were subjected to  $20 \text{ cm s}^{-1}$  southwest currents.

The second flood was not preceded by a low water period but was accompanied by a strong Mistral wind and the SNL was directed southeast with a mean velocity of  $30 \text{ cm s}^{-1}$  according to the ADCP current profile. Wave-induced BSS of  $2 \text{ N m}^{-2}$  suspended bottom sediments and currents carried them southwest at a velocity of  $10 \text{ cm s}^{-1}$ .

In addition, the regular and slow decrease of the bottom layer height from mid-December to mid-February in the absence of any environmental event was probably the result of early diagenesis. This process creates a compaction of the most superficial sediments and pore-waters are thus released, reducing bottom layer porosity.

November and December 2006 floods brought 456 kT of sediments to the Mediterranean Sea with 256 kT (56%) deposited on a  $2 \text{ km}^2$  area on the prodelta. They led to the discharge of 7.7 GBq of  $^{137}\text{Cs}$  by the Rhône River towards the sea, 3.1 GBq (39.7%) of which were deposited on the studied area. The BSS entailed caused the suspension of 62 to  $100 \text{ kg m}^{-2}$  of sediments and 930 to  $1500 \text{ Bq m}^{-2}$  of  $^{137}\text{Cs}$ .

Episodes of Mistral winds generally do not affect the BNL but have a significant effect on SNL, although southeast winds induced waves suspend sediments. Considerable erosion occurred on February 18, 2007 due to high BSS ( $5 \text{ N m}^{-2}$ ) and was followed by the transport of eroded sediments southwest along the  $70 \text{ cm s}^{-1}$  bottom currents. The February, 18, 2007 storm generated suspension of  $4.7 \text{ T m}^{-2}$  of sediments and  $70.7 \text{ kBq m}^{-2}$  of  $^{137}\text{Cs}$ . The distance of sediment transport

1 during flood and storm events can be estimated from between several metres above the water-  
2 sediment interface to several kilometres at the air-water interface. Rhône River radionuclides  
3 bound to suspended sediments are sometimes found in the northwest part of the Gulf of Lions  
4 (Roussiez, 2006).  
5  
6  
7  
8  
9

## 10 **5. Conclusion**

11  
12  
13 During the winter of 2006-2007, the Rhône River catchment area was affected by two moderate  
14 flood events, fed by rainfalls originating from the Cevennes Mountains on November 18, 2006 and  
15 from the ocean on December 9, 2006. Water flows reached  $3775 \text{ m}^3 \text{ s}^{-1}$  and  $3520 \text{ m}^3 \text{ s}^{-1}$  in  
16 Beaucaire and caused the suspension and transport of substantial amounts of sediment to the  
17 Rhône prodelta.  
18  
19  
20  
21  
22  
23

24  
25 Suspended sediment fluxes, forced by waves, river flow and local currents, were directed  
26 southwest. Their deposition, depending on settling velocity, flocculation and the direction of  
27 currents in the water column, varied with location on the prodelta.  
28  
29  
30  
31

32  
33 The coarsest and most of the flocculated grains settle near the river mouth, forming the muddy-  
34 sandy bar (4-5 m beneath the water surface). More distally, the BNL, fed by silty-clay sediments  
35 that aggregated in the water column by contact with salt water, were present and exhibited a  
36 muddy carpet. According to the ADCP data, the SNL (flood plume) moved seawards,  
37 progressively following currents and particles sinking mechanisms.  
38  
39  
40  
41  
42  
43

44  
45 The two floods provided a total quantity of sediment 11 cm thick in less than a month but erosion  
46 phases caused by southeast waves removed the deposits. BSS of  $1 \text{ to } 2 \text{ N m}^{-2}$  involved the  
47 suspension of bottom particles (mean diameter  $15 \text{ }\mu\text{m}$ ) that were then globally transported  
48 southwest.  
49  
50  
51  
52  
53

54  
55 This study has also enabled us to observe the erosional effects of southeast waves ( $H_s > 1.5 \text{ m}$ ),  
56 generating BSS up to  $5 \text{ N m}^{-2}$ , and the depositional effects of Rhône river inputs due to high flows  
57 ( $Q > 3000 \text{ m}^3 \text{ s}^{-1}$ ). While occurring at the same time, high waves and discharges alternate their  
58 effects and the BBI increases strongly, resulting in high suspended sediments concentrations. The  
59  
60  
61  
62  
63  
64  
65

1  
2  
3  
4  
5  
6  
7  
8  
9  
10  
11  
12  
13  
14  
15  
16  
17  
18  
19  
20  
21  
22  
23  
24  
25  
26  
27  
28  
29  
30  
31  
32  
33  
34  
35  
36  
37  
38  
39  
40  
41  
42  
43  
44  
45  
46  
47  
48  
49  
50  
51  
52  
53  
54  
55  
56  
57  
58  
59  
60  
61  
62  
63  
64  
65

annual sediment accumulation rate is probably in the range of 20 cm y<sup>-1</sup> to 50 cm y<sup>-1</sup>, but an important part of the sediment inputs are suspended by waves: only 40% of the radionuclides and 56% of the sediments supplied by the Rhône River deposit on a 2 km<sup>2</sup> area of the prodelta very close to the river mouth.

<sup>7</sup>Be and <sup>234</sup>Th<sub>xs</sub> activity-depth profiles traced recent flood deposition and enabled two events to be distinguished. Sediment layers 3 to 3.5 cm thick and 2 to 9.5 cm thick deposited during the March and the November-December floods. Grain-size distribution seems to be a good proxy to show the impact of recent high energy events like floods but is not efficient for setting their limits.

## Acknowledgements

This publication is a part of the CARMA project, including the marine staff of the LERCM (Laboratory of Environmental Radioecology in the Continental and Marine areas) at the IRSN and the geomorphology team of the CEREGE, notably C. Vassas and S. Meulé. The CARMEX campaign would not have been possible without the crew of the vessel “RV L’Europe” and the instrumentation was assisted by the IN VIVO and ADHOC VISION societies. We also thank S. Charmasson, J. Miralles and F. Bourrin for their advices, A. Jaffrenou for processing some core samples and X. Durrieu de Madron for lending us instruments.

## References

- Allison, M.A., Sheremet, A., Goni, M.A., Stone, G.W., 2005. Storm layer deposition on the Mississippi-Atchafalaya subaqueous delta generated by Hurricane Lili in 2002. *Continental Shelf Research*, 25, 2213-2232.
- Aloisi, J.C, Monaco, A., 1975. La sédimentation infra-littorale. Les prodeltas nord- méditerranéens. *C. R. Acad. Sc. D.280*, 2833-2836.

- 1  
2  
3  
4  
5  
6  
7  
8  
9  
10  
11  
12  
13  
14  
15  
16  
17  
18  
19  
20  
21  
22  
23  
24  
25  
26  
27  
28  
29  
30  
31  
32  
33  
34  
35  
36  
37  
38  
39  
40  
41  
42  
43  
44  
45  
46  
47  
48  
49  
50  
51  
52  
53  
54  
55  
56  
57  
58  
59  
60  
61  
62  
63  
64  
65
- Antonelli, C., Eyrolle, F., Rolland, B., Provansal, M., Sabatier, F., 2008. Suspended sediment and  $^{137}\text{Cs}$  fluxes during the exceptional December 2003 flood in the Rhone River, southeast France. *Geomorphology* 95, 350-360.
- Appleby, P.G., Oldfield, F., Thomson, R., Huttunen, P., Tolonen, K., 1979.  $^{210}\text{Pb}$  dating of annually laminated lake sediments from Finland. *Nature*, 280, 53-55.
- Ardhuin, F., Bertotti, L., Bidlot, J.-R., Cavaleri, L., Filipetto, V., Lefevre, J.-M., Wittmann, P., 2007. Comparison of wind and wave measurements and models in the Western Mediterranean Sea. *Ocean Engineering* 34 (3-4), 526-541
- Arnaud-Fassetta, G., 2003. River channel changes in the Rhône Delta (France) since the end of the Little Ice Age: geomorphological adjustment to hydroclimatic change and natural resource management. *Catena*, 51, 141-172.
- Bouisset, P., Calmet, D., 1997. Hyper Pure gamma-ray spectrometry applied to low-level environmental sample measurements. *International Workshop on the Status of Measurement Techniques for the Identification of Nuclear Signatures*, Geel, pp. 73-81.
- Bourrin, F., Durrieu de Madron, X., Ludwig, W., 2006. Contribution to the study of coastal rivers and associated prodeltas to sediment supply in the Gulf of Lions (NW Mediterranean). *Vie et milieu – Life and Environment*, 56 (4), 307-314.
- Bourrin, F., Monaco, A., Aloisi, J.C., Sanchez-Cabeza, J.A., Lofi, J., Heussner, S., Durrieu de Madron, X., Jeanty, G., Buscail, R., Saragoni, G., 2007. Last millenia sedimentary record on a micro-tidal, low accumulation prodelta (Têt river). *Mar. Geol.*, 243 (1-4), 77-96.
- Calmet, D., et Fernandez, J.M., 1990. Caesium distribution in the northwest Mediterranean seawater, suspended particles and sediment. *Continental Shelf Research*, 10, 895-913.
- Canuel, E.A., Martens, C.S., Benninger, L.K., 1990. Seasonal variations in  $^7\text{Be}$  activity in the sediments of Cape Lookout Bight, North Carolina. *Geochim. Cosmochim. Acta* 54, 237-245.
- Charmasson, S., 1998. Cycle du combustible nucléaire et milieu marin. Devenir des effluents rhodaniens en Méditerranée et des déchets immergés en Atlantique Nord-Est. *Rapport CEA-R-5826*, 70-74.

- 1 Charmasson, S., Bouisset P., Radakovitch O., Pruchon A.S., Arnaud M., 1998. Long-core profiles of  
2  $^{137}\text{Cs}$ ,  $^{134}\text{Cs}$ ,  $^{60}\text{Co}$  and  $^{210}\text{Pb}$  in sediment near the Rhône River (Northwestern Mediterranean  
3 Sea). *Estuaries*, 21, 3, 367-378.
- 4 Charmasson, S., 2003. Caesium 137 inventory in sediment near the Rhone mouth : role played by  
5 different sources. *Oceanologica Acta* 26, 435-441.
- 6  
7  
8  
9  
10 Chu, P.C., Qi, Y., Chen, Y., Shi, P., Mao, Q., 2004. South China sea wind-wave characteristics. Part I:  
11 validation of Wavewatch III using TOPEX/Poseidon data. *Journal of atmospheric and oceanic*  
12 *technology* 21, 1718-1733.
- 13  
14  
15  
16  
17 Corbett, D.R., Dail, M., McKee, B., 2007. High-frequency time-series of the dynamic sedimentation  
18 processes on the western shelf of the Mississippi River Delta. *Continental Shelf Research*, 27,  
19 1600-1615.
- 20  
21  
22  
23  
24 Corbett, D.R., McKee, B., Duncan, D., 2004. An evaluation of mobile mud dynamics in the  
25 Mississippi River deltaic region. *Mar. Geol.*, 209, 91-112.
- 26  
27  
28  
29 Curran, K.J., Hill, P.S., Milligan, T.G., 2002. Fine-grained suspended sediment dynamics in the Eel  
30 River flood plume. *Continental Shelf Research*, 22, 2537-2550.
- 31  
32  
33  
34 Curran, K.J., Hill, P.S., Milligan, T.G., Mikkelsen, O.A., Law, B.A., Durrieu de Madron, X., Bourrin,  
35 F., 2007. Settling velocity, effective density, and mass composition of suspended sediment in a  
36 coastal bottom boundary layer Gulf of Lions, France. *Continental Shelf Research*, 27, 1408-1421.
- 37  
38  
39  
40  
41 Drexler, T.M., Nittrouer, C.A., 2008. Stratigraphic signatures due to flood deposition near the Rhône  
42 River: Gulf of Lions, northwest Mediterranean Sea. *Continental Shelf Research*, 28, 1877-1894.
- 43  
44  
45  
46 Dufois, F., 2008. Modélisation du transport particulaire dans le Golfe du Lion: premières applications  
47 au devenir des traceurs radioactifs. Thèse de doctorat à l'Université de Toulon, 380 pp.
- 48  
49  
50  
51 Eyrolle, F., Rolland, B., Antonelli, C., 2006. Artificial radioactivity within the Rhone river waters –  
52 Consequences of flood on activity levels and fluxes toward the sea. *Environnement, Risques et*  
53 *Santé* 5, 2, 83-92.
- 54  
55  
56  
57  
58 Fain, A.M.V., Ogston, A.S., Sternberg, R.W., 2007. Sediment transport event analysis on the western  
59 Adriatic continental shelf. *Continental Shelf Research*, 27, 431-451.
- 60  
61  
62  
63  
64  
65



- 1  
2  
3  
4  
5  
6  
7  
8  
9  
10  
11  
12  
13  
14  
15  
16  
17  
18  
19  
20  
21  
22  
23  
24  
25  
26  
27  
28  
29  
30  
31  
32  
33  
34  
35  
36  
37  
38  
39  
40  
41  
42  
43  
44  
45  
46  
47  
48  
49  
50  
51  
52  
53  
54  
55  
56  
57  
58  
59  
60  
61  
62  
63  
64  
65
- Fox, J.M., Hill, P.S., Milligan, T.G., Boldrin, A., 2004. Flocculation and sedimentation on the Po River delta. *Mar. Geol.*, 203, 95-107.
- François, R.E., Garrison, G.R., 1982. Sound absorption based upon ocean measurement, part ii. *J. Acoust. Soc. of Am.*, 72(6), 1870-1890.
- Frignani, M., Langone, L., Ravaioli, M., Sorgente, D., Alvisi, F., Albertazzi, S., 2005. Fine-sediment mass balance in the western Adriatic continental shelf over a century time scale. *Mar. Geol.*, 222-223, 113-133.
- Frignani, M., Sorgente, D., Langone, L., Albertazzi, S., Ravaioli, M., 2004. Behaviour of Chernobyl radiocaesium in sediments of the Adriatic Sea off the Po River delta and the Emilia-Romagna coast. *J. Environ. Radioact.* 71, 299-312.
- Gillette, D.A., Blifford, I.H., Fenster, C.R., 1972. Measurements of the aerosols size distribution and vertical fluxes of aerosols on land subject to wind erosion. *J. Appl. Meteorol.* 11, 977-987.
- Guerra, J.V., Ogston, A.S., Sternberg, R.W., 2006. Winter variability of physical processes and sediment-transport events on the Eel River shelf, northern California. *Continental Shelf Research*, 26, 2050-2072.
- Guillén, J., Bourrin, F., Palanques, A., Durrieu de Madron, X., Puig, P., Buscail, R., 2006. Sediment dynamics during „wet’ and „dry’ storm events on the Têt inner shelf (SW Gulf of Lions). *Mar. Geol.*, 234, (1-4), 452-474.
- He, Q., and Walling, D.E., 1996. Interpreting particle size effects in the adsorption of  $^{137}\text{Cs}$  and unsupported  $^{210}\text{Pb}$  by mineral soils and sediments. *J. Environ. Radioact.*, 30 (2), 117-137.
- Heussner, S., Durrieu de Madron, X., Calafat, A., Canals, M., Carbonne, J., Delsaut, N., Saragoni, G., 2006. Spatial and temporal variability of downward particle fluxes on a continental slope: lessons from an 8-year experiment in the Gulf of Lions (NW Mediterranean). *Mar. Geol.*, 234, (1-4), 63-92.
- Jestin, H., Bassoullet, P., Le-Hir, P., L’Havanc, J., Degres, Y., 1998. Development of ALTUS, a high frequency acoustic submersible recording altimeter to accurately monitor bed elevation and

quantify deposition or erosion of sediments. In: Proceedings of Ocean'98-IEEC/OES Conference, Nice (France), pp. 189–194.

Kuelh, S.A., Nittrouer, C.A., Allison, M.A., Faria, L.E.C., Dukat, D.A., Jaeger, J.M., Pacioni, T.D., Figueiredo, A.G., Underkoffler, E.C., 1995. Sediment deposition, accumulation, and seabed dynamics in an energetic fine-grained coastal environment. *Continental Shelf Research*, 16, 5/6, 787-815.

Lansard, B., 2005. Distribution et remobilisation du plutonium dans les sédiments du prodelta du Rhône (Méditerranée Nord-Occidentale). Thèse de doctorat, pp. 180.

Lansard, B., Grenz, C., Charmasson, S., Schaaff, E., Pinazo, C., 2006. Potential plutonium remobilisation linked to marine sediment resuspension: first estimates based on flume experiments. *Journal of Sea Research*, 55, 74-85.

Law, B.A., Hill, P.S., Milligan, T.G., Curran, K.J., Wiberg, P.L., Wheatcroft, R.A., 2008. Size sorting of the fine-grained sediments during erosion: results from the western Gulf of Lions. *Continental Shelf Research*, 28 (15), 1935-1946.

Maillet, G., Vella, C., Berné, S., Friend, P., Amos, C., Fleury, T., Normand, A., 2006. Morphological changes and sedimentary processes induced by the December 2003 flood event at the present mouth of the Grand Rhône River (Southern France). *Mar. Geol.*, 234, 159-177.

Maréchal, J.C., Ladouche, B., Dörflinger, N., 2006. Role of karst system in the genesis of flash flood events in the Nîmes city. EGU 2006, Geophysical Research Vol.8, 06173, 2006.

Milligan, T.G., Hill, P.S., Law, B.A., 2007. Flocculation and the loss of sediment from the Po River plume. *Continental Shelf Research*, 27, 309-321.

Miralles, J., Arnaud, M., Radakovitch, O., Marion, C., Cagnat, X., 2006. Radionuclide deposition in the Rhône River Prodelta (NW Mediterranean Sea) in response to the December 2003 extreme flood. *Mar. Geol.*, 234, 179-189.

Miralles, J., Radakovitch, O., Aloisi, J.C., 2005.  $^{210}\text{Pb}$  sedimentation rates from the Northwestern Mediterranean margin. *Mar. Geol.*, 216, 155-167.

- 1  
2  
3  
4  
5 Monaco, A., Biscaye, P.E., Pocklington, R., 1990. France-JGOFS, ECOMARGE, Particle fluxes and  
6 ecosystem response on a continental margin: the mediterranean experiment. *Continental Shelf*  
7 *Research*, 10, 9-11.  
8  
9 Monaco, A., Durrieu de Madron, X., Radakovitch, O., Heussner, S., Carbone, J., 1999. Origin and  
10 variability of downward biogeochemical fluxes on the Rhône continental margin (NW  
11 Mediterranean). *Deep Sea Research I* 46, 1483-1511.  
12  
13 Moore, W.S., DeMaster, D.J., Smoak, J.M., McKee, B.A., Swarzenski, P.W., 1995. Radionuclide  
14 tracers of sediment-water interactions on the Amazon shelf. *Continental Shelf Research*, 16, 5/6,  
15 645-665.  
16  
17 Naudin, J.J., Cauwet, G., Chrétiennot-Dinet, M.J., Deniaux, B., Devenon, J.L., Pauc, H., 1997. River  
18 discharge and wind influence upon particulate transfer at the land-ocean interaction : case study of  
19 the Rhône River plume. *Estuar. Coast. Shelf Science*, 45, 303-316.  
20  
21 Nittrouer, C.A., De Master, D.J., McKee, B.A., Cutshall, N.H., Larsen, I.L., 1983/1984. The effect of  
22 sediment mixing on Pb-210 accumulation rates for the Washington continental shelf. *Mar. Geol.*,  
23 54, 201-221.  
24  
25 Nittrouer, C.A., De Master, D.J., 1986. Sedimentary processes on the Amazon continental shelf: past,  
26 present and future research. *Cont. Shelf Research* 6, 5-30.  
27  
28 Nittrouer, C.A., Kuelh, S.A., Sternberg, R.W., Figueiredo, Jr A.G., Faria, L.E.C., 1995. An  
29 introduction to the geological significance of sediment transport and accumulation on the Amazon  
30 continental shelf. *Mar. Geol.*, 125, 177-192.  
31  
32 Palanques, A., Durrieu de Madron, X., Puig, P., Fabres, J., Guillén, J., Calafat, A, Canals, M.,  
33 Heussner, S., Bonnin, J., 2006. Suspended sediment fluxes and transport processes in the Gulf of  
34 Lions submarine canyons. The role of storms and dense water cascading. *Mar. Geol.*, 234 (1-4),  
35 43-61.  
36  
37 Palinkas, C.M., Nittrouer, C.A., 2007. Modern sediment accumulation on the Po shelf, Adriatic Sea.  
38 *Continental Shelf Research*, 27, 489-505.  
39  
40  
41  
42  
43  
44  
45  
46  
47  
48  
49  
50  
51  
52  
53  
54  
55  
56  
57  
58  
59  
60  
61  
62  
63  
64  
65

- 1  
2  
3  
4  
5  
6  
7  
8  
9  
10  
11  
12  
13  
14  
15  
16  
17  
18  
19  
20  
21  
22  
23  
24  
25  
26  
27  
28  
29  
30  
31  
32  
33  
34  
35  
36  
37  
38  
39  
40  
41  
42  
43  
44  
45  
46  
47  
48  
49  
50  
51  
52  
53  
54  
55  
56  
57  
58  
59  
60  
61  
62  
63  
64  
65
- Palinkas, C.M., Nittrouer, C.A., Wheatcroft, R.A., Langone, L., 2005. The use of  $^7\text{Be}$  to identify event and seasonal sedimentation near the Po River delta, Adriatic Sea. *Mar. Geol.* 222-223, 95-112.
- Pauc, H., 2005. Formation of the Aude, Orb and Herault prodeltas and their characterisation using physicochemical and sedimentological parameters. *Mar. Geol.*, 222-223, 335-343.
- Pont, D., Simonnet, J.P., Walter, A.V, 2002. Medium-terms changes in suspended sediment delivery to the ocean: consequences of catchment heterogeneity and river management (Rhône river, France). *Estuar. Coast. Shelf Sci.* 54, 1-18.
- Radakovitch, O., Charmasson, S., Arnaud, M., Bouisset, P., 1999.  $^{210}\text{Pb}$  and caesium accumulation in the Rhône delta sediments. *Estuar. Coast. Shelf Sci.* 48, 77-92.
- Radakovitch, O., Roussiez, V., Ollivier, P., Ludwig, W., Grenz, C., Probst, J.L., 2008. Input of particulate heavy metals from rivers and associated sedimentary deposits on the Gulf of Lions continental shelf. *Estuar. Coast. Shelf Sci.*, 77 (2), 285-295.
- Rolland, B., 2006. Transfert des radionucléides artificiels par voie fluviale : conséquences sur les stocks sédimentaires rhodaniens et les exports vers la Méditerranée. Thèse de doctorat, pp. 280.
- Roussiez, V., Aloisi, J.C., Monaco, A., Ludwig, W., 2005. Early muddy deposits along the Gulf of Lions shoreline: a key for a better understanding of the land-to-sea transfer of sediments and associated pollutant fluxes. *Mar. Geol.*, 222-223, 345-358.
- Roussiez, V., 2006. Les éléments métalliques: traceurs de la pression anthropique et du fonctionnement hydro-sédimentaire du Golfe du Lion. Thèse de doctorat à l'Université de Perpignan, 130 pp.
- Sabatier, P., Maillet, G., Provansal, M., Fleury, T.J., Suanez, S., Vella, C., 2006. Sediment budget of the Rhône delta shoreface since the middle of the 19<sup>th</sup> century. *Mar. Geol.*, 234, 143-157.
- Serrat, P., Ludwig, W., Navarro, B., Blazi, J.L., 2001. Variabilité spatio-temporelle des flux de matières en suspension d'un fleuve côtier méditerranéen : la Têt (France). *Earth and Planetary Sciences*, 333, 389-397.
- Sommerfield, C.K., Nittrouer, C.A., 1999. Modern accumulation rates and a sediment budget for the Eel shelf: a flood-dominated depositional environment. *Mar. Geol.*, 154, 227-241.

- 1  
2  
3  
4  
5  
6  
7  
8  
9  
10  
11  
12  
13  
14  
15  
16  
17  
18  
19  
20  
21  
22  
23  
24  
25  
26  
27  
28  
29  
30  
31  
32  
33  
34  
35  
36  
37  
38  
39  
40  
41  
42  
43  
44  
45  
46  
47  
48  
49  
50  
51  
52  
53  
54  
55  
56  
57  
58  
59  
60  
61  
62  
63  
64  
65
- Soulsby, R.L., 1997. Dynamics of marine sands. A manual for practical applications. 249 pp., Thomas Telford, London.
- Sternberg, R.W., Cacchione, D.A., Paulson, B., Kineke, G.C., Drake, D.E., 1996. Observations of sediment transport on the Amazon subaqueous delta. *Continental Shelf Research* 16, 697-715.
- Swart, D.H., 1974. Offshore sediment transport and equilibrium beach profiles. Delft Hydraulics Laboratory publication, 131.
- Syvitski, J.P.M., Kettner, A.J., Corregiari, A., Nelson, B.W., 2005. Distributary channels and their impact on sediment dispersal. *Mar. Geol.*, 222-223, 75-94.
- Tessier, C., 2006. Caractérisation et dynamique des turbidités en zone côtière : l'exemple de la région marine Bretagne Sud. Thèse de doctorat à l'Université de Bordeaux I n°3307. 400p.
- Thill, A., Moustier, S., Garnier, J.M., Estournel, C., Naudin, J.J., Bottero, J.Y., 2001. Evolution of particle size and concentration in the Rhône river mixing zone: influence of salt flocculation. *Continental Shelf Research*, 21 (2127-2140).
- Thomas, A.J., 1997. Input of artificial radionuclides to the Gulf of Lions and tracing the Rhône influence in marine surficial sediments. *Deep Sea Research II*, 44, 577-595.
- Tolman, H.L., 2002a. User manual and system documentation of WAVEWATCH-III version 2.22. Tech. report 222, NOAA/NWS/NCEP/MMAB.
- Wheatcroft, R.A., Drake, D.E., 2003. Post-depositionnal alteration and preservation of sedimentary event layers on continental margins, I. The role of episodic sedimentation. *Mar. Geol.*, 199, 123-137.
- Weaver, P.P.E., Canals, M., Trincardi, F., 2006. EUROSTRATAFORM: special issue of *Marine Geology*. *Mar. Geol.*, 234, (1-4), 1-2.
- Zuo, Z., Eisma, D., Gieles, R., Beks, J., 1996. Accumulation rates and sediment deposition in the northwestern Mediterranean. *Deep Sea Research*, 44, 3-4, 597-609.

1  
2  
3  
4  
5  
6  
7  
8  
9  
10  
11  
12  
13  
14  
15  
16  
17  
18  
19  
20  
21  
22  
23  
24  
25  
26  
27  
28  
29  
30  
31  
32  
33  
34  
35  
36  
37  
38  
39  
40  
41  
42  
43  
44  
45  
46  
47  
48  
49  
50  
51  
52  
53  
54  
55  
56  
57  
58  
59  
60  
61  
62  
63  
64  
65

Fig. 1: Bathymetric map of the Grand Rhône River mouth. Dots represent the cores sampling stations.

Fig. 2: Water flows of upstream (a) and downstream (b) Rhône tributaries during the floods of Nov. and Dec. 2006. (CNR).

Fig. 3 : ADCP data recovered in the whole water column close to the Roustan Est buoy (current directions in degrees (a); current velocity in  $\text{cm s}^{-1}$  (b); turbidity in dB (c)), sedimentation evolution in cm next to the Roustan Est buoy (d), winds direction and intensity in  $\text{m s}^{-1}$  (e), Rhône River flow in  $\text{m}^3 \text{s}^{-1}$  measured in Beaucaire (f), swell direction in degrees (spots) and height in m (curve) at the Rhône River mouth (g).

Fig. 4: Current velocity in  $\text{cm s}^{-1}$  and direction (sticks) in the whole water column from 1.5 mab near the Roustan Est buoy.

Fig. 5: Volumic retrodiffusion index (BBI) in dB 1.5 m above the bottom (a), bottom shear stress in  $\text{N m}^{-2}$  due to: the currents (b), the waves (c), the currents and the waves (d).

Fig. 6: Rhône River flow in  $\text{m}^3 \text{s}^{-1}$  between the end of the altimeter record and the core sampling time.

Fig. 7: Mean grain sizes in micrometers (top) and grain-size vertical distribution (bottom) in the USHC20, USC30, USC20 and US04Kb cores sampled during the CARMEX campaign.

Fig. 8: Vertical radionuclides activities ( $^{137}\text{Cs}$ ,  $^7\text{Be}$ ,  $^{234}\text{Th}$ ,  $^{210}\text{Pb}$ ) in  $\text{Bq kg}^{-1}$  dry weight in the USHC20 (left), USC30 (center) and USC20 (right) cores sampled during the CARMEX campaign.

## In situ record of sedimentary processes near the Rhône River mouth during winter events (Gulf of Lions, Mediterranean Sea)

Marion C.<sup>1,2</sup>, Dufois F.<sup>2,3</sup>, Arnaud M.<sup>2</sup>, Vella C.<sup>4</sup>,

<sup>1</sup> University of Perpignan, 52 avenue Paul Alduy, 66860 Perpignan Cedex, France

<sup>2</sup> IRSN, DEI/SESURE Centre Ifremer, BP 330, 83507 La Seyne-sur-Mer, France

<sup>3</sup> IFREMER, Centre de Brest, BP 70, 29280 Plouzané, France

<sup>4</sup> CEREGE, Europôle de l'Arbois, BP 80, 13545 Aix-en-Provence cedex 04, France

E-mail: [cedric.marion83@gmail.com](mailto:cedric.marion83@gmail.com)

Phone number: +33(0)667110893

### Abstract

The environment is impacted by natural and anthropogenic disturbances that occur at different spatial and temporal scales, and that lead to major changes and even disequilibria when exceeding the resiliency capacities of the ecosystem. With an annual mean flow of  $1700 \text{ m}^3 \text{ s}^{-1}$ , the Rhône River is the largest of the western Mediterranean basin. Its annual solid discharges vary between 2 and 20 Mt, with flood events responsible for more than 70% of these amounts.

In the marine coastal area, close to the mouth, both flocculation and aggregation lead to the formation of fine-grained deposits, i.e. the prodelta. This area is characterized by sediment accumulation rates up to  $20\text{-}50 \text{ cm y}^{-1}$  and high accumulations of particle reactive contaminants such as various man-made radionuclides released into the river by nuclear facilities or arising from prior atmospheric nuclear tests (1954-1980) and the Chernobyl accident (April 1986). This prodelta, however, cannot be considered as a permanent repository for particle reactive pollutants since it is subjected to reworking processes.

Sediment dynamics had to be linked to the influences of hydrodynamic and atmospheric events such as high flow rates or storms close to the Rhône River mouth. An experiment was carried out during the winter 2006 based on the deployment of two ADCPs and six altimeters at the Grand Rhône mouth for several months. This type of installation has never been used before in this area because of the hard meteorological conditions and the strong fishing activities. However, results showed pluricentimetric rises of the

1  
2  
3  
4  
5  
6  
7  
8  
9  
10  
11  
12  
13  
14  
15  
16  
17  
18  
19  
20  
21  
22  
23  
24  
25  
26  
27  
28  
29  
30  
31  
32  
33  
34  
35  
36  
37  
38  
39  
40  
41  
42  
43  
44  
45  
46  
47  
48  
49  
50  
51  
52  
53  
54  
55  
56  
57  
58  
59  
60  
61  
62  
63  
64  
65

sedimentary level just after river flood events and decreases during storms, generated by southeast winds. Radiotracers and grain size depth profiles helped to characterise the studied events and to establish inventories of sediments and radionuclides. A cruise (CARMEX) was carried out during this same period to collect water samples, suspended particles and sediment cores. The results enabled us to link both river flow and wind characteristics to events recorded on the sea floor, i.e. resuspension, accumulation, consolidation, etc. Deposits of 11 cm of sediments were estimated during flood periods and bottom shear stresses up to 5 N m<sup>-2</sup> were calculated during sediment erosion phases.

**Keywords:** sediment dynamics, floods, hydrodynamics, radiotracers, Rhône River prodelta.

## 1. Introduction

Sediment dynamics in the Gulf of Lions have been studied in the framework of various projects (Ecomarge, Euromarge, Mater, US-Eurostrataform and EU-Eurostrataform (Monaco et al., 1990; Weaver et al., 2006)). These projects have led to a better understanding of sediment pathways from their sources, i.e. rivers, to their deposits in deltas, shelves, canyons and eventually to deep basins (Heussner et al., 2006; Palanques et al., 2006). The Gulf of Lions is especially interesting since it is a river-dominated continental shelf fed primarily by the Rhône River and also by several coastal rivers such as the Vidourle, Lez, Herault, Orb, Aude, Agly, Têt and Tech (Bourrin et al., 2006). For the past several years, monitoring has been implemented on different rivers, in particular the Têt River (Serrat et al., 2001) and the Rhône River in the western and the eastern part of the Gulf, respectively. These monitoring programmes have confirmed that most of the sediment fluxes from rivers occurred during flood events such as those recorded in 1994, 2002 and 2003 (Antonelli et al., 2008; Rolland, 2006; Miralles et al., 2006).

Sedimentary processes near river mouths have been the subject of many studies for the past several decades throughout the world, especially for the most important bodies such as the Mississippi River (Allison et al, 2005; Corbett et al., 2004, 2007), the Amazon (Nittrouer and DeMaster, 1986; Nittrouer et al, 1995; Kuelh et al., 1995; Moore et al., 1995; Sternberg, 1996), the Eel River (Sommerfield et al., 1999; Curran et al., 2002; Wheatcroft and Drake, 2003; Guerra et al., 2006),



1  
2  
3  
4  
5  
6  
7  
8  
9  
10  
11  
12  
13  
14  
15  
16  
17  
18  
19  
20  
21  
22  
23  
24  
25  
26  
27  
28  
29  
30  
31  
32  
33  
34  
35  
36  
37  
38  
39  
40  
41  
42  
43  
44  
45  
46  
47  
48  
49  
50  
51  
52  
53  
54  
55  
56  
57  
58  
59  
60  
61  
62  
63  
64  
65

and the Po (Fox et al., 2004; Syvitski et al., 2005; Palinkas et al., 2005, 2007; Fain et al., 2007; Milligan et al., 2007). For the Gulf of Lions, these processes have been studied in the framework of the Eurostrataform programme, primarily in the Têt prodelta (Guillén et al., 2006; Law et al., 2008); whereas the Rhône system has not received the same attention until now.

The prodeltas of these rivers (Pauc, 2005) have been shown to be efficient traps for river-borne sediments and associated contaminants (Charmasson, 1998; Radakovitch et al., 1999; Charmasson, 2003; Roussiez et al., 2005). However, these areas can not be considered as final repositories because resuspension, remobilisation and displacement processes of sediments and particle-bound elements are expected, due to the effects of waves and currents (Lansard et al., 2006; Radakovitch et al., 2008). In these shallow waters, it is thus important to quantify the processes of sediment dynamics in relation to physical forcing linked to high energy events such as floods and storms (Bourrin et al., 2007).

A project (CARMA, french acronym for Consequences of Rhône River Inputs to the Associated Coastal Environnement) was thus implemented and this publication presents results obtained during the winter 2006-2007. The aims of this first event-response survey were: i) to characterise storm/discharge events and, ii) evaluate their relationship with sedimentation and erosion records in the Rhône prodelta area by means of different tools like radiotracers, iii) calculate the inventories of sediments and  $^{137}\text{Cs}$  on a part of the prodelta. The goal is also to follow the impact of extreme meteorological events on the prodelta sedimentary bed thanks to the installation of autonomous instruments, which had not been used until now in the study area.

### *1.1. The local setting*

With a catchment area of 95,500 km<sup>2</sup> and a mean flow-rate of 1700 m<sup>3</sup> s<sup>-1</sup>, the Rhône river is the main source of water and sediments in the western Mediterranean Sea. The river is 814 km long with its source in the Alps. As described by Arnaud-Fassetta et al. (2003), it crosses many different environnements and has varied during time with the different climatic periods. Its mouth opens

1 onto a prodelta that receives annual amounts of particles between 2 and 20 Mt (Sabatier et al.,  
2 2006; Eyrolle et al, 2006; Pont et al, 2002).

3 This subaqueous prodelta (30 km<sup>2</sup>) is composed of coarse grains comprising sands (> 63µm)  
4 forming sandy bars, and of fine grains constituted of clays (< 4µm) and silts (4 µm to 63 µm)  
5 (Aloisi and Monaco, 1975).  
6  
7

8  
9 The area chosen for instrument deployment in the framework of the CARMA project is very  
10 close to the Grand Rhône River mouth (Fig. 1), on the prodelta, at the boundary with the  
11 Camargues marshes on the west and the oil industry of Fos-sur-mer (Bouches-du-Rhône) on the  
12 east. Here the level of risk was considered acceptable for positioning permanent instrumentation.  
13  
14

15 The estuary is not considered to be influenced by Mediterranean Sea tides (microtidal), even if  
16 several centimetres high, but primarily by marine currents and swells. In addition, depending on  
17 their directions and intensities, superficial and bottom currents play different roles, e.g. suspension  
18 transport, erosion, deposition, etc. (Naudin et al., 1997; Maillet et al., 2006). Winds have  
19 considerable effects on hydrodynamics and sediment transport.  
20  
21  
22  
23  
24  
25  
26  
27  
28  
29  
30

### 31 32 33 34 *1.2. Flood events* 35 36

37 Because of its size, the Rhône valley is subject to different kinds of floods: mediterranean,  
38 oceanic, cevenol and generalised (Rolland, 2006). On December 4, 2003, an exceptional flood  
39 occurred with maximum river discharge reaching 11500 m<sup>3</sup> s<sup>-1</sup> in Arles. Because of the rapidity of  
40 the water rise (nearly 8000 m<sup>3</sup> s<sup>-1</sup> in 30 h, according to Antonelli et al. (2008), dykes burst and the  
41 banks broke, leading to large masses of solid suspended matter being carried over.  
42  
43  
44  
45  
46  
47  
48

49 Flood events are therefore important for the supply of material to the coastal area: it was estimated  
50 that the Rhône River releases 80% of the annual amount of sediments in several days of flooding  
51 (Rolland, 2006). At the same time, floods discharge tremendous amounts of radionuclides.  
52 Antonelli et al. (2008) calculated that  $77 \pm 16$  GBq of <sup>137</sup>Cs were released by the Rhône River  
53 during the exceptional flood (December 2003), although Rolland (2006) found an amount of 158  
54 GBq (48.7%) during the entire year 2003. Miralles et al. (2006) estimated that  $75 \pm 21$  GBq of  
55  
56  
57  
58  
59  
60  
61  
62  
63  
64  
65

1  
2  
3  
4  
5  
6  
7  
8  
9  
10  
11  
12  
13  
14  
15  
16  
17  
18  
19  
20  
21  
22  
23  
24  
25  
26  
27  
28  
29  
30  
31  
32  
33  
34  
35  
36  
37  
38  
39  
40  
41  
42  
43  
44  
45  
46  
47  
48  
49  
50  
51  
52  
53  
54  
55  
56  
57  
58  
59  
60  
61  
62  
63  
64  
65

$^{210}\text{Pb}$  in excess of its background ( $^{210}\text{Pb}_{\text{xs}}$ ) and  $27 \pm 2$  GBq of  $^{137}\text{Cs}$  were deposited during the flood of December 2003. Radioactive tracers can be used to follow sedimentary masses and enable to calculate sediment accumulation rates near the Rhône River mouth.

### 1.3. *Wind stress*

Two main types of winds affect the studied area. They are either originated from north, called Mistral, or from south-east, called Marin, and can be very strong during several days. The first one is channelized in the Rhône River valley and delivers cold air. The second one comes from offshore and is responsible of high waves generation.

## 2. Material and methods

The CARMA project started in September 2006 with the immersion of the first instruments in the Grand Rhône River mouth, near the Roustan Est buoy, and terminated by the CARMEX campaign in March 2007 (Fig. 1).

### 2.1. *Seabed and currents monitoring*

The results detailed here are from a S-ALTUS altimeter located near the Roustan Est buoy at a depth of 18 m. It was placed 64 cm above the bottom and recorded its distance to the floor every 15 minutes. The principle relies on the emission/reception of an acoustic beam by a cylindrical sensor during 30 ms with a frequency of 2 MHz (Jestin et al, 1998). The accuracy and resolution of the ALTUS were respectively 0.41 mm and 2 mm.

In addition, a RDI<sup>TM</sup> Workhorse Sentinel Acoustic Doppler Current Profilers (ADCP) was also immersed at 18 m depth right of the river mouth at the Roustan Est buoy. The transducers emitted 600 kHz beams and received an acoustic signal which frequency was different due to Doppler Effect.

1  
2  
3  
4  
5  
6  
7  
8  
9  
10  
11  
12  
13  
14  
15  
16  
17  
18  
19  
20  
21  
22  
23  
24  
25  
26  
27  
28  
29  
30  
31  
32  
33  
34  
35  
36  
37  
38  
39  
40  
41  
42  
43  
44  
45  
46  
47  
48  
49  
50  
51  
52  
53  
54  
55  
56  
57  
58  
59  
60  
61  
62  
63  
64  
65

Since the ADCP was set at 50 cmab, therefore the first available data was located 155 cmab. The ADCP yielded current data every 18 seconds and averaged them every 15 minutes along 40 depth cells 50 cm high, with an accuracy of  $0.51 \text{ cm s}^{-1}$ . Backscattering was measured by an electric signal as counts, transformed into an energy balance in decibels, linking the emission and reception levels of the acoustic wave. MATLAB was used to correct the attenuation effects of interfering parameters such as the water column (model of François and Garrison, 1982; Tessier, 2006), near field correction factor (Downing formulation), propagation length and the air-water interface. These backscattering values in dB, however, are relative and cannot be compared to other backscattering data from other ADCPs. They qualitatively show backscattering variations, linked to turbidity, during this period. Unfortunately, not enough suspended sediment matter (SSM) concentrations were measured so as to calibrate the ADCP data precisely but a calibration has been estimated thanks to samples from the CARMEX campaign in March 2007 (Dufois, 2008).

## 2.2. *Waves and winds modelling*

35  
36  
37  
38  
39  
40  
41  
42  
43  
44  
45  
46  
47  
48  
49  
50  
51  
52  
53  
54  
55  
56  
57  
58  
59  
60  
61  
62  
63  
64  
65

The ALADIN atmospheric meso-scale model of Météo-France shows the wind conditions in the Grand Rhône River mouth area ( $43.3^\circ \text{ N}$ ,  $4.8^\circ \text{ E}$ ). Each node of the grid in this area is separated by 3 km. This weather profile covered the entire study period, showing the wind intensity and direction. Wave fields were modelled in the western Mediterranean Sea with a resolution of  $0.1^\circ$  using the third generation WAVEWATCH-III wind-wave model (Tolman, 2002a) forced by Météo-France wind fields. This model, developed at NOAA/NCEP and adapted from the WAM model, has been successfully applied in global- and regional-scale studies in many areas throughout the world's oceans (Chu et al., 2004), in particular in the western Mediterranean Sea (Ardhuin et al., 2007). The model is based on the two-dimensional wave action balance equation including energy density generation and dissipation terms by wind, white-capping, wave-bottom interaction, and redistribution of wave energy due to wave-wave interactions. The model was

validated and compared to other models for two periods in 2002 and 2003 (Ardhuin et al., 2007) and in 2001 (Dufois, 2008).

The current-induced bottom shear stress BSS ( $\tau_c$ ) was calculated with the assumption that the velocity profile is logarithmic down to the first layer of the ADCP above the bottom:

$$\tau_c = \rho u_{*c}^2 \text{ with } u_{*c} = \frac{\kappa u(z)}{\ln(z/z_0)} \quad (1)$$

where  $\rho$  is water density,  $\kappa$  the Von Karman constant (=0.4),  $z$  the height of the first layer above the bottom,  $u(z)$  the associated velocity and  $z_0$  the bed roughness. Since the sediment is cohesive in this area,  $z_0$  was set at 0.1 mm, a typical value found in the literature (Soulsby, 1997).

For the wave-induced BSS ( $\tau_w$ ) we used the usual formulation, which depends on orbital velocity  $U_b$  just above the bed:

$$\tau_w = 0.5 \rho f_w U_b^2 \quad (2)$$

with (Swart, 1974)  $f_w=0.3$  if  $A/k_s < 1.57$ ,

$$\text{and beyond: } f_w = 0.00251 \exp(5.21(A/k_s)^{-0.19}), \quad (3)$$

where  $A$  is the orbital half-excursion near the bottom ( $A = \frac{U_b T}{2\pi}$ ,  $T$  being the wave period).

The total BSS was calculated by direct addition of wave-induced BSS and the current-induced BSS without taking non-linear wave-current interactions into account.

### *2.3. Radionuclide geochronology and particle size: sampling and analyses*

Four of the nine sediment cores sampled during the CARMEX cruise (March 11-17, 2007, RV L'Europe) were analysed for their grain size distribution and/or to estimate sediment accumulation rates in this area. US04Kb was sampled close to the instruments location, USCh30 and USCh20 in channel-like structures, while USHCh20 was located nearby but out of these bottom structures. They were sub-sampled twice using circular Plexiglas tubes (18 cm diameter, 50 cm long) in box-cores collected by USNEL (large volume box-corer) carefully maintaining the sediment-water interface undisturbed. The length of the cores varied from 34 to 40 cm and their sampling depths

1 were 22 to 49 m on the continental shelf. These cores were sliced in 1 cm sections. Each 1 cm  
2 thick sediment layer was dried, crushed, passed through a 200  $\mu\text{m}$  sieve and put in 200 mL and 60  
3 mL geometries for gamma spectrometry investigations. These analyses were conducted at the  
4 IRSN laboratory in Orsay, near Paris, with N-type hyper-purity germanium detectors in 200 mL  
5 volume containers and measured with a counting time of 20 or 40 h. Efficiency calibrations from  
6 22.5 keV to 1.8 keV were carried out using mixed gamma-ray sources in a solid resin-water  
7 equivalent matrix with a density of 1.15  $\text{g cm}^{-3}$  (Bouisset et Calmet, 1997). Activity results were  
8 corrected for true coincidence summing and self-absorption effects.  $^7\text{Be}$ ,  $^{137}\text{Cs}$ ,  $^{210}\text{Pb}$  and  $^{234}\text{Th}$   
9 were determined.

10  $^7\text{Be}$  ( $t_{1/2}=53.2$  d) is a natural radionuclide, resulting from the cosmic ray spallation of nitrogen and  
11 carbon in the atmosphere. It was analysed in order to determine particulate deposit up to 200 days  
12 and even more. It settles on the river-bed, bounds to detritic particles and spreads in marine  
13 systems via river discharges (Canuel et al., 1990). Palinkas et al. (2005) suggested to perform  
14 several sedimentological analyses to confirm the short-time-scale sediment accumulation rates  
15 found with  $^7\text{Be}$ .

16  $^{137}\text{Cs}$  ( $t_{1/2}=30.1$  y) is an anthropogenic radionuclide and originated from nuclear tests, nuclear  
17 accidents such as Chernobyl in April 1986, and nuclear power plant discharges, i.e. the spent fuel  
18 reprocessing site at Marcoule. It has a high affinity for clays and fine particles in fresh water and  
19 has been found to be a good tracer of the Rhône River inputs to the Gulf of Lions.  $^{137}\text{Cs}$  depth  
20 profiles have been extensively used in various environments to assess sediment accumulation rates,  
21 notably coupled with  $^{210}\text{Pb}_{\text{xs}}$  (Appleby et al., 1979; Nittrouer et al., 1983/1984; He and Walling,  
22 1995; Radakovitch et al., 1999; Frignani et al., 2004).

23  $^{210}\text{Pb}$  ( $t_{1/2}=22.3$  y) is a naturally occurring radionuclide produced in soil, sediment and water by the  
24 decay in the atmosphere of  $^{226}\text{Ra}$  through its daughter  $^{222}\text{Rn}$ . The cycle ends in lacustrine and  
25 marine sediments where two types of  $^{210}\text{Pb}$  can be found: that produced in situ (called supported)  
26 and that coming with the accumulated particles (called unsupported or excess). Because of its

specific half-life, excess  $^{210}\text{Pb}$  ( $^{210}\text{Pb}_{\text{xs}}$ ), calculated by removing  $^{214}\text{Pb}$  to total  $^{210}\text{Pb}$ , is useful for assessing centennial sediment accumulation rates in marine systems (Miralles et al., 2005).

$^{234}\text{Th}$  ( $t_{1/2}=24.1$  d) is a radiogenically produced radionuclide, arising from the decay of  $^{238}\text{U}$  dissolved in seawaters. Due to its high affinity for particles, it is soon delivered to sediments and its short half-life enables particulate dynamics and sedimentation to be assessed during flood events. Also in this case, the dating parameter is in excess ( $^{234}\text{Th}_{\text{xs}}$ ) over the fraction produced in situ.

Radionuclide activities were corrected for the decay over the time elapsed between sampling and counting. Furthermore,  $^{137}\text{Cs}$  depth profiles do not show any dating feature because of the length of the sediment cores, the low activities and the absence of the end of the signal.

An aliquot of fresh sediment from each layer was kept for grain-size characterisation, using a Beckmann & Coulter LS 13320 laser grain sizer, with multi-wavelength technology called Polarization Intensity Differential Scattering (PIDS) enabling a better accuracy for clay fractions.

Fresh sediments were placed in 5 cL plastic tubes and diluted with water to obtain a concentration close to  $10 \text{ g L}^{-1}$ . Ten mL of these solutions were analysed with the laser grain sizer. Three replicates were analysed for each sample and were averaged to verify the quality of the results. The range of analysis was  $0.4 \mu\text{m}$  to  $2000 \mu\text{m}$  with an accuracy of 3% for median size and 5% for each side of the distribution profile. Five ranges have been used to classify the grain sizes: clays ( $<4 \mu\text{m}$ ), fine silts (4 to  $20 \mu\text{m}$ ), coarse silts (20 to  $63 \mu\text{m}$ ), fine sands (63 to  $200 \mu\text{m}$ ) and coarse sands ( $>200 \mu\text{m}$ ). Values of D10, D50 and D90 were calculated, representing respectively the maximum diameter of 10%, 50% and 90% of the sediment samples.

Inventories were obtained thanks to ArcGIS® and Surfer® softwares, processing data from the sediment cores sampled during CARMEX with interpolation methods.

### 3. Results

#### 3.1. Rhône River flow rate

Fig. 2a and Fig. 2b show water flows of the Rhone River (at the Beaucaire station, just upstream from the separation between the Grand Rhône River and the Petit Rhône River) and of its upstream tributaries (Isère, Gard, Ardèche, Saône, Perrache, Cèze, Ouvèze). Flood threshold ( $3000 \text{ m}^3 \text{ s}^{-1}$ ) was exceeded in Beaucaire on November 18, 2006 ( $3775 \text{ m}^3 \text{ s}^{-1}$ ) and on December 9, 2006 ( $3520 \text{ m}^3 \text{ s}^{-1}$ ). These flows are likely to provide enough sediment to significantly impact the prodelta and to the Gulf of Lions.

The increased flow rate in Beaucaire and at the Rhône river mouth on November 18, 2006 resulted from an increase in the flow-rates of the Cèze, Gard and Ardèche rivers (Fig. 2b), which are Cevenol rivers, reaching values three times their flood discharge thresholds and with a return period lower than 2 years. The origin of this high Rhône river flow was undoubtedly a Cevenol flash flood (Maréchal, 2006; Antonelli et al., 2008). On the contrary, the flood of December 9 is of oceanic type. In this case, the entire catchment area undergoes an increase of water flow: upstream rivers multiply their mean flows by a factor of 6 and downstream rivers from 3- to 5- fold (Fig. 2a).

#### 3.2. Wind conditions

Several episodes of violent and cold northerly winds (the Mistral) occurred during the study period, with velocities reaching  $20 \text{ m s}^{-1}$ . This Mistral was in fact the strongest wind ever recorded here and the most frequent between November 8, 2006 and February 22, 2007. Some southeast winds blew in from the sea, creating turbulence on surface waters. They reached  $20 \text{ m s}^{-1}$  and considerably increased turbidity (Fig. 3b and Fig. 3e), combined with high river flow. These winds create a swell when they are continuously active during a quite long time (Fig. 3e and Fig. 3g) whereas long periods of Mistral winds do not cause considerable swells. In fact, winds from the north (between  $300^\circ\text{N}$  and  $50^\circ\text{N}$ ) cause no or only weak swells, with heights less than one metre.



1 Southerly and easterly winds from the Mediterranean Sea, however, caused an increase in swell  
2 formation, especially from mid-November to mid-December 2006 and on February 18, 2007 when  
3 a swell peak reached a height of 3 m.  
4  
5  
6

### 7 *3.3. Data recorded in situ*

8  
9

10 Fig. 3 (a,b,c) shows current velocities and directions recorded near the Roustan Est buoy and the  
11 backscattered signal in the water column from November 8, 2006 to February 22, 2007. Superficial  
12 currents were primarily in the southwest direction until December 13, 2006. When the wind  
13 changed direction (Fig. 3e), i.e. a southeast wind was replaced by a north wind (Mistral); currents  
14 then changed direction, toward the southeast. In any case, no clear stratification appeared on  
15 profiles, since orientation was practically unchanged in the entire water column. On the contrary,  
16 velocity decreased with depth. The primary reason is that the currents induced were caused by  
17 winds, not by density variations.  
18  
19  
20  
21  
22  
23  
24  
25  
26  
27  
28  
29

30 On November 18, 2006, current velocities (Fig. 3b), reached  $50 \text{ cm s}^{-1}$  and did not change very  
31 much with depth ( $30 \text{ cm s}^{-1}$ , 1.5 mab). At the same time, the ADCP recorded a backscattered signal  
32 of 90 dB. Higher values of backscattering were recorded (100 dB) on November 20, 2006, related  
33 to a southeast (SE) wind velocity of  $8 \text{ m s}^{-1}$ . The period of SE winds was characterised by swell  
34 waves, causing bottom shear stress. Swell heights peaked (Fig. 6g) on November 20 (1.8 m),  
35 December 9, 2006 (1.9 m), January 24 (2 m) and February 18, 2007 (2.9 m) increasing the  
36 backscattering signal (80 to 100 dB).  
37  
38  
39  
40  
41  
42  
43  
44  
45  
46

47 The second flood period (December 9, 2006) occurred while Mistral winds were blowing at a  
48 velocity of  $15 \text{ m s}^{-1}$ , despite a short episode of SE winds. In general, northerly winds are more  
49 intense than southeast winds but they need to last in time to induce bottom shear stress. The  
50 backscattered signal high level lasted for 4 days, corresponding to the increased flow-rate.  
51  
52  
53  
54  
55  
56  
57  
58  
59  
60  
61  
62  
63  
64  
65

1  
2  
3  
4  
5  
6  
7  
8  
9  
10  
11  
12  
13  
14  
15  
16  
17  
18  
19  
20  
21  
22  
23  
24  
25  
26  
27  
28  
29  
30  
31  
32  
33  
34  
35  
36  
37  
38  
39  
40  
41  
42  
43  
44  
45  
46  
47  
48  
49  
50  
51  
52  
53  
54  
55  
56  
57  
58  
59  
60  
61  
62  
63  
64  
65

more than 5 m beneath the water surface, for 5 days. They caused an important swelling (Fig. 3g) and resulted in the settling of suspended particles and the resuspension of bottom sediment, as shown in Fig. 3c.

On January 24, 2007, the peak in swell height (2 m) was concomitant with an increase in Rhône River flow ( $2200 \text{ m}^3 \text{ s}^{-1}$ ) leading to an acceleration of the surface currents (nearly  $80 \text{ cm s}^{-1}$ ). Similarly, on February 18, 2007 the series of highest waves of the study was recorded (2.9 m) during strong SE winds ( $20 \text{ m s}^{-1}$ ) together with an increase in flow-rate ( $2500 \text{ m}^3 \text{ s}^{-1}$ ) leading to relatively constant southwest current velocity ( $> 60 \text{ cm s}^{-1}$ ) in the water column (Fig. 4).

### 3.4. Sediment characteristics

Core US04Kb, taken from a site close to the position of the instruments (Fig. 1), shows a mean grain diameter of  $15.3 \mu\text{m}$ , i.e. the size of fine silts, when averaging the topmost 5 cm (Fig. 7). The core was composed of 15 % of clays, 70 % of silts and 15 % of sands. These values are characteristics of the entire prodelta area (Radakovitch et al, 1999; Miralles et al., 2006).

Fig. 3d shows the distance between the altimeter transducer and the prodelta bottom during the study period. The net balance in deposition/erosion processes between November 2006 and February 2007 is almost zero. Nevertheless, important changes occurred on a shorter time scale. These changes appear to be linked to changes in environmental conditions recorded in parallel. It is to be stressed that several „blank’ periods in Fig. 3d, were due to very high SSM concentrations or something that temporarily interfered with the transducer beam.

The quantitative understanding of these records requires calculation of the BSS occurred during our experiment and link their values to sediment suspension and erosion (Fig. 5).

Series of waves, combined with currents, created a succession of BSS between  $1.5$  and  $2 \text{ N m}^{-2}$  and, as a consequence, Bottom Backscattering Indices (BBI), related to suspended solid concentrations, were close to 70 to 80 dB. The greatest BBI, approaching 100 dB, occurred during strong water flows (more than mean liquid discharge) but considerable BSS also increased BBI.

1  
2  
3  
4  
5  
6  
7  
8  
9  
10  
11  
12  
13  
14  
15  
16  
17  
18  
19  
20  
21  
22  
23  
24  
25  
26  
27  
28  
29  
30  
31  
32  
33  
34  
35  
36  
37  
38  
39  
40  
41  
42  
43  
44  
45  
46  
47  
48  
49  
50  
51  
52  
53  
54  
55  
56  
57  
58  
59  
60  
61  
62  
63  
64  
65

Two periods of accretion appeared on the altimetric profile of Fig. 3d, exactly during or just after the high Rhône River discharges. The first deposition time D1 occurred on November 18 and increased the bottom level by 5 cm in less than 3 days: the distance between the transducer and the floor (DTF) decreased from 63.5 cm to 58.5 cm. The second deposition time D2 occurred on November 9, 2006, and reduced the DTF by 6 cm (62 cm to 56 cm) in 9 days. The D1 event corresponded to a flow increase of nearly  $3000 \text{ m}^3 \text{ s}^{-1}$  in 36 h and a flood duration of 24 h, while the D2 event corresponded to a flow increase of  $2300 \text{ m}^3 \text{ s}^{-1}$  in 6 days and a flood duration of 3 days. Between these two deposition phases, an erosion phase E1 removed at least 4.5 cm of sediment, probably due to a succession of high BSS values (Fig. 5).

On February 18, 2007, almost 4 cm of sediment disappeared in only several hours during an erosive event E2. At this time, both  $15 \text{ m s}^{-1}$  SE winds with 3 m high waves and Rhône river flow around  $2500 \text{ m}^3 \text{ s}^{-1}$  induced  $60 \text{ cm s}^{-1}$  bottom currents oriented southeast and a BSS of  $5 \text{ N m}^{-2}$ . The latter was due primarily to waves (90%) and led to peak values reaching 93 dB in BBI (Fig. 5a).

No special event was recorded during the second half of December, a month characterised primarily by compaction processes and early diagenesis.

A thin deposition on January 3, 2007, confirmed by BBI of 90 dB, appeared just after an increase in water flow of  $1300 \text{ m}^3 \text{ s}^{-1}$ .

On January 24, 2007, inputs from the Rhône River (flows higher than  $2000 \text{ m}^3 \text{ s}^{-1}$ ) and the strong influence of waves (BSS of  $2.6 \text{ N m}^{-2}$ ) caused increases of the backscattered signal in the water column (Fig. 3c) and the bottom layer (Fig. 5a), with no intense accretion or erosion recorded (Fig. 3d). Except for these two January events, the mid-December to mid-February period characterised by both low river discharges and wave effects, the water-sediment interface remained regular and almost flat.

Cores sampled during the oceanographic campaign, i.e. almost 17 days after the last data recorded in situ (Fig. 6), showed that fine fractions (clays and silts) were prevailing but more sands were recently deposited (Fig. 7).

1 Station US04Kb was the closest to the mooring, at a distance of 100 m and a depth of 25 m. Layers  
2 3 cm thick with 10% coarse sand appeared at the water-sediment interface, whereas the sandy  
3 component downcore (ca. 10%) was finer. This shows a recent, substantial and sudden input.

4 CNR (french acronym of National Company of the Rhône River) data, obtained from  
5 continuously recording of sediment hydrodynamic times, showed a flood event just before the core  
6 sampling time (Fig. 6). Altimeter data proved that Rhône river discharges more than  $3000 \text{ m}^3 \text{ s}^{-1}$ ,  
7 even with wave effects, caused deposit of sediments. The fraction of coarse grains was probably  
8 due to this increase of river flow, since absolute bottom depth remained constant from November  
9 8, 2006, to February 22, 2007. This third flood event reached an average flow peak of  $3667.2 \text{ m}^3 \text{ s}^{-1}$   
10 and remained above the  $3000 \text{ m}^3 \text{ s}^{-1}$  threshold for one week. It seems to have been the origin of  
11 the deposit of 3 to 5 cm of sandy sediments close to the Rhône river mouth. The fact that three  
12 high flow events succeeded each other and that they were synchronous with successions of high  
13 waves, did not enable the sandy layers to deposit for a long time and be covered by fine grain  
14 sediments. There is thus no very definite peak of coarse sands in the different cores but some thin  
15 layers appear.

### 35 *3.5. Sediments accumulation*

36 Apparent sediment accumulation rates were roughly calculated in three cores collected just in  
37 front of the Rhône River mouth (USChenal20m, USChenal30m and USHChenal20m) using  
38 radiotracer activity depth distributions (Fig. 8).  $^{137}\text{Cs}$  and  $^{210}\text{Pb}_{\text{xs}}$  profiles are strongly correlated.  
39 However, due to the end of reprocessing operations in Marcoule,  $^{137}\text{Cs}$  activities are quite low  
40 compared to the values observed before 1997 (Charmasson, 1998).  $^{137}\text{Cs}$  values ranged from 3.1  
41  $\text{Bq kg}^{-1}$  to  $16.5 \text{ Bq kg}^{-1}$  in the three cores. Their  $^{137}\text{Cs}$  inventories were  $8900 \text{ Bq.m}^{-2}$ ,  $7604 \text{ Bq.m}^{-2}$   
42 and  $8470 \text{ Bq.m}^{-2}$ , respectively.

43 Total radioactivities of  $^{210}\text{Pb}$  (also for  $^{210}\text{Pb}_{\text{xs}}$ ) varied according the same change of  $^{137}\text{Cs}$ : signal  
44 increases and decreases occurred at the same depth. Concentrations ranged from 31.2 to  $118 \text{ Bq}$   
45  $\text{kg}^{-1}$  in the three cores. Their  $^{210}\text{Pb}_{\text{xs}}$  inventories were  $53647 \text{ Bq.m}^{-2}$ ,  $67604 \text{ Bq.m}^{-2}$  and  $61347$

1 Bq.m<sup>-2</sup>, respectively. USC20 and USC30 are two channel-like stations which apparently  
2 accumulated more radionuclides than USHC20, as shown by comparing the activity ranges. This  
3 can result from the fact that channel-like structures are preferential pathways for sediments for all  
4 the size scales (canyons, channels).  
5

6  
7 Strong dilution signatures are not really visible on <sup>137</sup>Cs and <sup>210</sup>Pb<sub>xs</sub> profiles, in comparison with  
8 studies realised by Miralles et al. (2006) and Drexler et Nittrouer (2008) on Rhône River floods.  
9  
10 However, their flow rates were more important compared to our case.  
11

12  
13 The depth profiles of <sup>137</sup>Cs and <sup>210</sup>Pb are not suitable to calculate sediment accumulation rates.  
14  
15 None of the classical models for <sup>210</sup>Pb dating can be applied to this very dynamic environment,  
16  
17 due to episodic and inconstant delivery. However, <sup>7</sup>Be and <sup>234</sup>Th<sub>xs</sub> patterns permitted to estimate  
18  
19 recent sediment deliveries, by dividing the depth of the base of the profiles by 5 times the half lives  
20  
21 of the radionuclides.  
22  
23

24  
25  
26 The <sup>7</sup>Be signal ceases at 16, 14 and 10 cm depth in cores USC20, USC30 and USHC20,  
27  
28 respectively. The base of the <sup>7</sup>Be depth profile reflects the beginning of the accumulation of fresh  
29  
30 sediment, i.e. almost 200 days. USHC20 accumulated less sediment than the other cores, as  
31  
32 explained above. Integrated over the entire year, the calculated maximum sediment accumulation  
33  
34 rates are 29.2 cm y<sup>-1</sup>, 46.6 cm y<sup>-1</sup> and 53.3 cm y<sup>-1</sup> for USHC20, USC30 and USC20, respectively.  
35  
36

37  
38  
39 <sup>234</sup>Th<sub>xs</sub> signals disappear between 3 and 3.5 cm in each core but there were abrupt peaks at 5, 8 and  
40  
41 11 cm with intensities of 51.7, 152.4 and 154.5 Bq kg<sup>-1</sup>, for USHC20, USC30 and USC20,  
42  
43 respectively. These results would confirm that apparent sediment accumulation rate at USC20 is  
44  
45 slightly higher than at USC30 and much higher than at USHC20. Signals completely disappeared  
46  
47 at depths of 5.5, 11.5 and 13 cm, respectively. The first three centimetres were probably deposited  
48  
49 very recently, during the last flood (from March 3 to 10, 2007), as it is showed by the core  
50  
51 US04Kb. Nevertheless, the peaks would reflect that previous inputs of sediments occurred in  
52  
53 December and/or November 2006 (Fig. 8). In this case, maximum sediment accumulation rates  
54  
55 were estimated between 16.5 and 22 cm y<sup>-1</sup> for USHC20, between 34.5 and 46 cm y<sup>-1</sup> for USC30  
56  
57  
58  
59  
60  
61  
62  
63  
64  
65

and between 39 and 52 cm y<sup>-1</sup> for USC20. The sediment accumulation rates calculated using <sup>7</sup>Be and <sup>234</sup>Th<sub>xs</sub> are thus quite similar.

The decrease of hydrodynamics is evident in USHC20 at the depth of 11 cm, with a sandy fraction diminishing from more than 20% to less than 3% (along a 5 cm layer), and with D50 and D90 from 6 μm to 20 μm and from 20 μm to 120 μm, respectively (Fig. 7). A decrease in accumulation rate with consequent increase of <sup>210</sup>Pb<sub>xs</sub> activity is visible (Fig. 8). USHC20 revealed a 17 cm homogeneous layer (13.4 Bq kg<sup>-1</sup> and 99.5 Bq kg<sup>-1</sup> for <sup>137</sup>Cs and <sup>210</sup>Pb<sub>xs</sub>), followed by a decrease (3.6 Bq kg<sup>-1</sup> and 34.6 Bq kg<sup>-1</sup>) and then an increase (12.6 Bq kg<sup>-1</sup> and 69 Bq kg<sup>-1</sup>) at 29 cm beneath the sediment surface for both <sup>137</sup>Cs and <sup>210</sup>Pb<sub>xs</sub>. USC20 and USC30 also show this pattern, even if it is not as well-defined as USHC20. Grain size and radiotracers concentrations signals are really concomitant and account for the April 2006 Rhône River flood (4164 m<sup>3</sup> s<sup>-1</sup>). Drexler et Nittrouer (2008) normalised the excess <sup>210</sup>Pb with the clay content to remove the effects related strictly to grain size. They observed a dilution signature in their <sup>210</sup>Pb<sub>xs</sub> profiles, accounting for an increase of the high river flow.

The end of the <sup>7</sup>Be signal corresponds to almost 200 days and to 100 days for <sup>234</sup>Th<sub>xs</sub> (Palinkas et al., 2005) and did not cease at the same depths. This would mean that the winter events (last 100 days) caused heterogeneous accumulation rates, although during the preceding 100 days, the ASR was constant according to 3 cores (from 3 to 4.5 cm). This can be explained by the fact that hydrology and meteorology parameters are totally different in summer/autumn and in winter/spring.

#### 4. Discussion

The results presented here show a very good correlation between all the parameters studied: currents, waves and wind directions and intensities, backscattered signals, river discharges and sedimentary phases, BSS and BBI. Deposition phases in fact occurred during the two flood events, erosion episodes occurred while waves effects were greatest and southeast winds were correlated with swell impacts and high BBI.

#### 4.1. Impact of storms

1 Bourrin et al. (2007) monitored the Têt prodelta during wet and dry storms, i.e. during strong  
2 wave events associated with high and low river flows. Accretion phases were observed during wet  
3 storms, while dry storms led to erosion phases. Mean discharges of the Têt and the Rhône rivers  
4 are different,  $10 \text{ m}^3 \text{ s}^{-1}$  and  $1700 \text{ m}^3 \text{ s}^{-1}$ , but sedimentary mechanisms occurring off their mouths  
5 are similar. The critical shear stresses causing erosion evaluated in the laboratory for the Têt and  
6 the Rhône coastal areas are different:  $0.12 \text{ N m}^{-2}$  (Guillén et al., 2006; Bourrin et al., 2007) and  
7 from  $0.068$  to  $0.087 \text{ N m}^{-2}$  (Lansard et al., 2006), respectively. These latter data would correspond  
8 to the suspension of the fluffy layer.  
9

10 Recent experiments on the Rhône prodelta evaluated critical BSS of  $0.35 \text{ N m}^{-2}$  (Dufois, 2008).  
11 BSS exceeded  $1 \text{ N m}^{-2}$  six times in three months of relatively quiet periods on the Rhône prodelta,  
12 but only twice on the Têt prodelta during the intense storms that occurred in December 2003 and in  
13 January 2004. Bottom currents were directed south and southwest in both river mouths during  
14 these events.  
15

16 Altimetric records showed alternately deposition/erosion phases (from days to weeks) and the  
17 balance over the studied period is zero. The Bottom Boundary Layer (BBL), responsible for  
18 sediment dispersion over the Gulf of Lions (Monaco et al., 1999; Lansard et al., 2006), is fed by  
19 sediments resuspension processes, forming the Benthic Nepheloid Layer (BNL).  
20

21 Law et al. (2008) asserted that individual grain size classes of the BNL are being eroded in  
22 proportions equal to the seabed and verified the sorting of bottom sediment size distributions  
23 across the Têt River mouth. Sandy fractions and mean grain sizes decrease in the seaward direction  
24 and with increasing depth. The results are comparable to the Rhône River mouth in USC20 (22 m)  
25 and USC30 (49 m): from 19.2% to 1.8% sands and D50 from  $18.7 \mu\text{m}$  to  $13.6 \mu\text{m}$  (Fig. 7).  
26  
27  
28  
29  
30  
31  
32  
33  
34  
35  
36  
37  
38  
39  
40  
41  
42  
43  
44  
45  
46  
47  
48  
49  
50  
51  
52  
53  
54  
55  
56  
57  
58  
59  
60  
61  
62  
63  
64  
65

## 4.2. Hydrodynamics

1       Lansard (2005) deployed an ADCP near the Rhône River mouth from April 29 to June 5, 2002.  
2  
3       The instruments did not record any flood but river flow and waves reached  $2700 \text{ m}^3 \text{ s}^{-1}$  (May 5)  
4  
5       and 1.8 m high (May 8). During peak flow, the ADCP recorded strong backscattered signals, the  
6  
7       direction of bottom currents was southwest during 55% of the study period and velocities were  
8  
9       higher than  $15 \text{ cm s}^{-1}$  86% of the time. These observations are consistent with the conditions of the  
10  
11       winter of 2006-2007.  
12  
13

14       The highest waves observed by Lansard (2005) were caused by southeast winds ( $90^\circ$  to  $180^\circ$ ) and  
15  
16       led to BSS of  $0.4 \text{ N m}^{-2}$ . This value was exceeded by the highest 11 BSS results recorded during  
17  
18       CARMA (with 5 events between  $1 \text{ N m}^{-2}$  and  $4.5 \text{ N m}^{-2}$ ). In agreement with the observations by  
19  
20       Lansard (2005), each BSS peak was accompanied by high BBI, showing the resuspension of  
21  
22       sediments after that critical erosion stress  $\tau_{\text{erosion}}$  was reached (established in a laboratory thanks to  
23  
24       flume experiments in a channel). The minimum and maximum  $\tau_{\text{erosion}}$  were estimated as  $0.08 \text{ N m}^{-2}$   
25  
26       and  $0.12 \text{ N m}^{-2}$  at the Roustan Est buoy. The current-induced BSS exceeded the maximum  $\tau_{\text{erosion}}$   
27  
28       ( $0.35 \text{ N m}^{-2}$ ) by three-fold and reached  $0.55 \text{ N m}^{-2}$  during the storm of January 24, 2007.  
29  
30  
31  
32  
33

34       In addition, two wave series were higher than 1.5 m in May 2002 compared to 8 wave series in the  
35  
36       winter of 2006-2007, representing 10% of the study period. Winter periods with high flood events  
37  
38       and strong storms (especially due to southeast winds), caused harsher environmental conditions for  
39  
40       the Rhône River than in spring.  
41  
42  
43  
44  
45  
46

## 4.3. Apparent sediment accumulation rates (ASR)

47  
48       The results are in agreement with Charmasson et al. (1998), who used  $^{137}\text{Cs}/^{134}\text{Cs}$  activity ratios  
49  
50       to estimate sediment accumulation rates in the prodelta that ranged from 37 to  $48 \text{ cm y}^{-1}$  at the  
51  
52       mouth by means of a several years study, and with Calmet and Fernandez (1990) with values of  
53  
54       30-35  $\text{cm y}^{-1}$ . Here,  $^{134}\text{Cs}$  is no more detectible preventing us from using  $^{137}\text{Cs}/^{134}\text{Cs}$  ratio to  
55  
56       calculate sedimentation rates (Charmasson et al., 1998; Radakovitch et al., 1999). The range  
57  
58  
59  
60  
61  
62  
63  
64  
65



1  
2  
3  
4  
5  
6  
7  
8  
9  
10  
11  
12  
13  
14  
15  
16  
17  
18  
19  
20  
21  
22  
23  
24  
25  
26  
27  
28  
29  
30  
31  
32  
33  
34  
35  
36  
37  
38  
39  
40  
41  
42  
43  
44  
45  
46  
47  
48  
49  
50  
51  
52  
53  
54  
55  
56  
57  
58  
59  
60  
61  
62  
63  
64  
65

evaluated is broad (from 29.2 to 53.3 cm y<sup>-1</sup> with <sup>7</sup>Be and from 16.5 to 52 cm y<sup>-1</sup> with <sup>234</sup>Th<sub>xs</sub>) because radionuclide concentrations were influenced by grain-size distributions. Radakovitch et al. (1999) obtained values higher than 20 cm y<sup>-1</sup> in the prodelta and 0.2 cm y<sup>-1</sup> over the shelf using the <sup>210</sup>Pb<sub>xs</sub> dating method and <sup>137</sup>Cs/<sup>134</sup>Cs activity ratios, confirmed by Zuo et al. (1996). Miralles et al. (2005) emphasised the difference between deposition in the Rhône River mouth (30-40 cm y<sup>-1</sup>) and the rest of the prodelta (0.65 cm y<sup>-1</sup>). Sedimentation rates strongly decrease with the distance from the river mouth.

According to published data, river mouths exhibit different ASRs: the Eel River with 0.4 cm y<sup>-1</sup> (Sommerfield et al., 1999) or 0.1 to 1 cm y<sup>-1</sup> (Wheatcroft and Drake, 2003), the Po River with 0.23 cm y<sup>-1</sup> (Palinkas et al., 2007) or 0.77 cm y<sup>-1</sup> (Frignani et al., 2005), the Amazon River with 10 to 60 cm y<sup>-1</sup> (Kuelh et al., 1995; Nitrouer et al., 1995), the Mississippi River with 2 cm y<sup>-1</sup> (Corbett et al., 2004) . Sediment accumulation rates are difficult to determine because physical (erosion, compaction, advection) and biogeochemical (bioturbation, early diagenesis, diffusion) processes interfere with radionuclide signals (Wheatcroft and Drake, 2003), and above all because of the high solid discharge variations at the river mouth.

#### 4.4. Fate of Rhône River inputs during the winter 2006-2007

During the two moderate floods periods, suspended sediments were carried southwest and south (Fig. 4) in the entire water column, with velocities decreasing with the depth. The coarsest particles deposited first near the mouth, feeding the sandy bar originated by the actions of the river and the waves. According to Thill (2001), during a low river discharge period (500 m<sup>3</sup> s<sup>-1</sup>), a saltwedge appears up to 20 km inland and is pushed seaward during a high river period (>2500 m<sup>3</sup> s<sup>-1</sup>). When fresh waters mix with salt waters, i) a portion of fine suspended sediment flocculates and settles to form larger entities contributing to the BNL (Curran et al., 2007) and ii) the remaining fraction moves seaward to form the Surface Nepheloid Layer (SNL) (Milligan et al., 2007). Other parameters/processes play a role in flocculation/deflocculation processes, such as organic matter contents, suspended sediment concentrations and particles-particles interactions.

1  
2  
3  
4  
5  
6  
7  
8  
9  
10  
11  
12  
13  
14  
15  
16  
17  
18  
19  
20  
21  
22  
23  
24  
25  
26  
27  
28  
29  
30  
31  
32  
33  
34  
35  
36  
37  
38  
39  
40  
41  
42  
43  
44  
45  
46  
47  
48  
49  
50  
51  
52  
53  
54  
55  
56  
57  
58  
59  
60  
61  
62  
63  
64  
65

Just before the first flood, Rhône River flow was between  $501 \text{ m}^3 \text{ s}^{-1}$  and  $560 \text{ m}^3 \text{ s}^{-1}$  for 2 days, causing the occurrence of a saltwedge and probably the flocculation of suspended particles. The 10 days following the first flood peak directed the SNL plume southwest with velocities reaching  $1 \text{ m s}^{-1}$ , although BSS resulting from waves and currents caused little suspension of BNL sediments ( $1 \text{ N m}^{-2}$ ). One day of weak northeast bottom circulation ( $15 \text{ cm s}^{-1}$ ) occurred during a long period of bottom southwest current velocities ranging from  $20 \text{ cm s}^{-1}$  to  $50 \text{ cm s}^{-1}$ . After this, both a wave-induced BSS of  $1.2 \text{ N m}^{-2}$  and the absence of river inputs enabled the erosion of the interface sediments, visible on the altimetric profile (November 26, 2006). While undergoing suspension, sediments were subjected to  $20 \text{ cm s}^{-1}$  southwest currents.

The second flood was not preceded by a low water period but was accompanied by a strong Mistral wind and the SNL was directed southeast with a mean velocity of  $30 \text{ cm s}^{-1}$  according to the ADCP current profile. Wave-induced BSS of  $2 \text{ N m}^{-2}$  suspended bottom sediments and currents carried them southwest at a velocity of  $10 \text{ cm s}^{-1}$ .

In addition, the regular and slow decrease of the bottom layer height from mid-December to mid-February in the absence of any environmental event was probably the result of early diagenesis. This process creates a compaction of the most superficial sediments and pore-waters are thus released, reducing bottom layer porosity.

November and December 2006 floods brought 456 kT of sediments to the Mediterranean Sea with 256 kT (56%) deposited on a  $2 \text{ km}^2$  area on the prodelta. They led to the discharge of 7.7 GBq of  $^{137}\text{Cs}$  by the Rhône River towards the sea, 3.1 GBq (39.7%) of which were deposited on the studied area. The BSS entailed caused the suspension of 62 to  $100 \text{ kg m}^{-2}$  of sediments and 930 to  $1500 \text{ Bq m}^{-2}$  of  $^{137}\text{Cs}$ .

Episodes of Mistral winds generally do not affect the BNL but have a significant effect on SNL, although southeast winds induced waves suspend sediments. Considerable erosion occurred on February 18, 2007 due to high BSS ( $5 \text{ N m}^{-2}$ ) and was followed by the transport of eroded sediments southwest along the  $70 \text{ cm s}^{-1}$  bottom currents. The February, 18, 2007 storm generated suspension of  $4.7 \text{ T m}^{-2}$  of sediments and  $70.7 \text{ kBq m}^{-2}$  of  $^{137}\text{Cs}$ . The distance of sediment transport

1 during flood and storm events can be estimated from between several metres above the water-  
2 sediment interface to several kilometres at the air-water interface. Rhône River radionuclides  
3 bound to suspended sediments are sometimes found in the northwest part of the Gulf of Lions  
4 (Roussiez, 2006).  
5  
6  
7  
8

## 9 **5. Conclusion**

10 During the winter of 2006-2007, the Rhône River catchment area was affected by two moderate  
11 flood events, fed by rainfalls originating from the Cevennes Mountains on November 18, 2006 and  
12 from the ocean on December 9, 2006. Water flows reached  $3775 \text{ m}^3 \text{ s}^{-1}$  and  $3520 \text{ m}^3 \text{ s}^{-1}$  in  
13 Beaucaire and caused the suspension and transport of substantial amounts of sediment to the  
14 Rhône prodelta.  
15  
16  
17  
18  
19  
20  
21  
22  
23  
24

25 Suspended sediment fluxes, forced by waves, river flow and local currents, were directed  
26 southwest. Their deposition, depending on settling velocity, flocculation and the direction of  
27 currents in the water column, varied with location on the prodelta.  
28  
29  
30  
31  
32

33 The coarsest and most of the flocculated grains settle near the river mouth, forming the muddy-  
34 sandy bar (4-5 m beneath the water surface). More distally, the BNL, fed by silty-clay sediments  
35 that aggregated in the water column by contact with salt water, were present and exhibited a  
36 muddy carpet. According to the ADCP data, the SNL (flood plume) moved seawards,  
37 progressively following currents and particles sinking mechanisms.  
38  
39  
40  
41  
42  
43  
44

45 The two floods provided a total quantity of sediment 11 cm thick in less than a month but erosion  
46 phases caused by southeast waves removed the deposits. BSS of  $1 \text{ to } 2 \text{ N m}^{-2}$  involved the  
47 suspension of bottom particles (mean diameter  $15 \text{ }\mu\text{m}$ ) that were then globally transported  
48 southwest.  
49  
50  
51  
52  
53

54 This study has also enabled us to observe the erosional effects of southeast waves ( $H_s > 1.5 \text{ m}$ ),  
55 generating BSS up to  $5 \text{ N m}^{-2}$ , and the depositional effects of Rhône river inputs due to high flows  
56 ( $Q > 3000 \text{ m}^3 \text{ s}^{-1}$ ). While occurring at the same time, high waves and discharges alternate their  
57 effects and the BBI increases strongly, resulting in high suspended sediments concentrations. The  
58  
59  
60  
61  
62  
63  
64  
65

1  
2  
3  
4  
5  
6  
7  
8  
9  
10  
11  
12  
13  
14  
15  
16  
17  
18  
19  
20  
21  
22  
23  
24  
25  
26  
27  
28  
29  
30  
31  
32  
33  
34  
35  
36  
37  
38  
39  
40  
41  
42  
43  
44  
45  
46  
47  
48  
49  
50  
51  
52  
53  
54  
55  
56  
57  
58  
59  
60  
61  
62  
63  
64  
65

annual sediment accumulation rate is probably in the range of 20 cm y<sup>-1</sup> to 50 cm y<sup>-1</sup>, but an important part of the sediment inputs are suspended by waves: only 40% of the radionuclides and 56% of the sediments supplied by the Rhône River deposit on a 2 km<sup>2</sup> area of the prodelta very close to the river mouth.

<sup>7</sup>Be and <sup>234</sup>Th<sub>xs</sub> activity-depth profiles traced recent flood deposition and enabled two events to be distinguished. Sediment layers 3 to 3.5 cm thick and 2 to 9.5 cm thick deposited during the March and the November-December floods. Grain-size distribution seems to be a good proxy to show the impact of recent high energy events like floods but is not efficient for setting their limits.

### Acknowledgements

This publication is a part of the CARMA project, including the marine staff of the LERCM (Laboratory of Environmental Radioecology in the Continental and Marine areas) at the IRSN and the geomorphology team of the CEREGE, notably C. Vassas and S. Meulé. The CARMEX campaign would not have been possible without the crew of the vessel “RV L’Europe” and the instrumentation was assisted by the IN VIVO and ADHOC VISION societies. We also thank S. Charmasson, J. Miralles and F. Bourrin for their advices, A. Jaffrenou for processing some core samples and X. Durrieu de Madron for lending us instruments.

### References

- Allison, M.A., Sheremet, A., Goni, M.A., Stone, G.W., 2005. Storm layer deposition on the Mississippi-Atchafalaya subaqueous delta generated by Hurricane Lili in 2002. *Continental Shelf Research*, 25, 2213-2232.
- Aloisi, J.C, Monaco, A., 1975. La sédimentation infra-littorale. Les prodeltas nord- méditerranéens. *C. R. Acad. Sc. D.280*, 2833-2836.

- 1  
2  
3  
4  
5  
6  
7  
8  
9  
10  
11  
12  
13  
14  
15  
16  
17  
18  
19  
20  
21  
22  
23  
24  
25  
26  
27  
28  
29  
30  
31  
32  
33  
34  
35  
36  
37  
38  
39  
40  
41  
42  
43  
44  
45  
46  
47  
48  
49  
50  
51  
52  
53  
54  
55  
56  
57  
58  
59  
60  
61  
62  
63  
64  
65
- Antonelli, C., Eyrolle, F., Rolland, B., Provansal, M., Sabatier, F., 2008. Suspended sediment and  $^{137}\text{Cs}$  fluxes during the exceptional December 2003 flood in the Rhone River, southeast France. *Geomorphology* 95, 350-360.
- Appleby, P.G., Oldfield, F., Thomson, R., Huttunen, P., Tolonen, K., 1979.  $^{210}\text{Pb}$  dating of annually laminated lake sediments from Finland. *Nature*, 280, 53-55.
- Ardhuin, F., Bertotti, L., Bidlot, J.-R., Cavaleri, L., Filipetto, V., Lefevre, J.-M., Wittmann, P., 2007. Comparison of wind and wave measurements and models in the Western Mediterranean Sea. *Ocean Engineering* 34 (3-4), 526-541
- Arnaud-Fassetta, G., 2003. River channel changes in the Rhône Delta (France) since the end of the Little Ice Age: geomorphological adjustment to hydroclimatic change and natural resource management. *Catena*, 51, 141-172.
- Bouisset, P., Calmet, D., 1997. Hyper Pure gamma-ray spectrometry applied to low-level environmental sample measurements. *International Workshop on the Status of Measurement Techniques for the Identification of Nuclear Signatures*, Geel, pp. 73-81.
- Bourrin, F., Durrieu de Madron, X., Ludwig, W., 2006. Contribution to the study of coastal rivers and associated prodeltas to sediment supply in the Gulf of Lions (NW Mediterranean). *Vie et milieu – Life and Environment*, 56 (4), 307-314.
- Bourrin, F., Monaco, A., Aloisi, J.C., Sanchez-Cabeza, J.A., Lofi, J., Heussner, S., Durrieu de Madron, X., Jeanty, G., Buscail, R., Saragoni, G., 2007. Last millenia sedimentary record on a micro-tidal, low accumulation prodelta (Têt river). *Mar. Geol.*, 243 (1-4), 77-96.
- Calmet, D., et Fernandez, J.M., 1990. Caesium distribution in the northwest Mediterranean seawater, suspended particles and sediment. *Continental Shelf Research*, 10, 895-913.
- Canuel, E.A., Martens, C.S., Benninger, L.K., 1990. Seasonal variations in  $^7\text{Be}$  activity in the sediments of Cape Lookout Bight, North Carolina. *Geochim. Cosmochim. Acta* 54, 237-245.
- Charmasson, S., 1998. Cycle du combustible nucléaire et milieu marin. Devenir des effluents rhodaniens en Méditerranée et des déchets immergés en Atlantique Nord-Est. *Rapport CEA-R-5826*, 70-74.

- 1 Charmasson, S., Bouisset P., Radakovitch O., Pruchon A.S., Arnaud M., 1998. Long-core profiles of  
2  $^{137}\text{Cs}$ ,  $^{134}\text{Cs}$ ,  $^{60}\text{Co}$  and  $^{210}\text{Pb}$  in sediment near the Rhône River (Northwestern Mediterranean  
3 Sea). *Estuaries*, 21, 3, 367-378.
- 4 Charmasson, S., 2003. Caesium 137 inventory in sediment near the Rhone mouth : role played by  
5 different sources. *Oceanologica Acta* 26, 435-441.
- 6  
7  
8  
9  
10 Chu, P.C., Qi, Y., Chen, Y., Shi, P., Mao, Q., 2004. South China sea wind-wave characteristics. Part I:  
11 validation of Wavewatch III using TOPEX/Poseidon data. *Journal of atmospheric and oceanic*  
12 *technology* 21, 1718-1733.
- 13  
14  
15  
16  
17 Corbett, D.R., Dail, M., McKee, B., 2007. High-frequency time-series of the dynamic sedimentation  
18 processes on the western shelf of the Mississippi River Delta. *Continental Shelf Research*, 27,  
19 1600-1615.
- 20  
21  
22  
23  
24 Corbett, D.R., McKee, B., Duncan, D., 2004. An evaluation of mobile mud dynamics in the  
25 Mississippi River deltaic region. *Mar. Geol.*, 209, 91-112.
- 26  
27  
28  
29 Curran, K.J., Hill, P.S., Milligan, T.G., 2002. Fine-grained suspended sediment dynamics in the Eel  
30 River flood plume. *Continental Shelf Research*, 22, 2537-2550.
- 31  
32  
33  
34 Curran, K.J., Hill, P.S., Milligan, T.G., Mikkelsen, O.A., Law, B.A., Durrieu de Madron, X., Bourrin,  
35 F., 2007. Settling velocity, effective density, and mass composition of suspended sediment in a  
36 coastal bottom boundary layer Gulf of Lions, France. *Continental Shelf Research*, 27, 1408-1421.
- 37  
38  
39  
40  
41 Drexler, T.M., Nittrouer, C.A., 2008. Stratigraphic signatures due to flood deposition near the Rhône  
42 River: Gulf of Lions, northwest Mediterranean Sea. *Continental Shelf Research*, 28, 1877-1894.
- 43  
44  
45  
46 Dufois, F., 2008. Modélisation du transport particulaire dans le Golfe du Lion: premières applications  
47 au devenir des traceurs radioactifs. Thèse de doctorat à l'Université de Toulon, 380 pp.
- 48  
49  
50  
51 Eyrolle, F., Rolland, B., Antonelli, C., 2006. Artificial radioactivity within the Rhone river waters –  
52 Consequences of flood on activity levels and fluxes toward the sea. *Environnement, Risques et*  
53 *Santé* 5, 2, 83-92.
- 54  
55  
56  
57  
58 Fain, A.M.V., Ogston, A.S., Sternberg, R.W., 2007. Sediment transport event analysis on the western  
59 Adriatic continental shelf. *Continental Shelf Research*, 27, 431-451.
- 60  
61  
62  
63  
64  
65

- 1  
2  
3  
4  
5  
6  
7  
8  
9  
10  
11  
12  
13  
14  
15  
16  
17  
18  
19  
20  
21  
22  
23  
24  
25  
26  
27  
28  
29  
30  
31  
32  
33  
34  
35  
36  
37  
38  
39  
40  
41  
42  
43  
44  
45  
46  
47  
48  
49  
50  
51  
52  
53  
54  
55  
56  
57  
58  
59  
60  
61  
62  
63  
64  
65
- Fox, J.M., Hill, P.S., Milligan, T.G., Boldrin, A., 2004. Flocculation and sedimentation on the Po River delta. *Mar. Geol.*, 203, 95-107.
- François, R.E., Garrison, G.R., 1982. Sound absorption based upon ocean measurement, part ii. *J. Acoust. Soc. of Am.*, 72(6), 1870-1890.
- Frignani, M., Langone, L., Ravaioli, M., Sorgente, D., Alvisi, F., Albertazzi, S., 2005. Fine-sediment mass balance in the western Adriatic continental shelf over a century time scale. *Mar. Geol.*, 222-223, 113-133.
- Frignani, M., Sorgente, D., Langone, L., Albertazzi, S., Ravaioli, M., 2004. Behaviour of Chernobyl radiocaesium in sediments of the Adriatic Sea off the Po River delta and the Emilia-Romagna coast. *J. Environ. Radioact.* 71, 299-312.
- Gillette, D.A., Blifford, I.H., Fenster, C.R., 1972. Measurements of the aerosols size distribution and vertical fluxes of aerosols on land subject to wind erosion. *J. Appl. Meteorol.* 11, 977-987.
- Guerra, J.V., Ogston, A.S., Sternberg, R.W., 2006. Winter variability of physical processes and sediment-transport events on the Eel River shelf, northern California. *Continental Shelf Research*, 26, 2050-2072.
- Guillén, J., Bourrin, F., Palanques, A., Durrieu de Madron, X., Puig, P., Buscail, R., 2006. Sediment dynamics during „wet’ and „dry’ storm events on the Têt inner shelf (SW Gulf of Lions). *Mar. Geol.*, 234, (1-4), 452-474.
- He, Q., and Walling, D.E., 1996. Interpreting particle size effects in the adsorption of  $^{137}\text{Cs}$  and unsupported  $^{210}\text{Pb}$  by mineral soils and sediments. *J. Environ. Radioact.*, 30 (2), 117-137.
- Heussner, S., Durrieu de Madron, X., Calafat, A., Canals, M., Carbonne, J., Delsaut, N., Saragoni, G., 2006. Spatial and temporal variability of downward particle fluxes on a continental slope: lessons from an 8-year experiment in the Gulf of Lions (NW Mediterranean). *Mar. Geol.*, 234, (1-4), 63-92.
- Jestin, H., Bassoullet, P., Le-Hir, P., L’Havanc, J., Degres, Y., 1998. Development of ALTUS, a high frequency acoustic submersible recording altimeter to accurately monitor bed elevation and

quantify deposition or erosion of sediments. In: Proceedings of Ocean'98-IEEC/OES Conference, Nice (France), pp. 189–194.

Kuelh, S.A., Nittrouer, C.A., Allison, M.A., Faria, L.E.C., Dukat, D.A., Jaeger, J.M., Pacioni, T.D., Figueiredo, A.G., Underkoffler, E.C., 1995. Sediment deposition, accumulation, and seabed dynamics in an energetic fine-grained coastal environment. *Continental Shelf Research*, 16, 5/6, 787-815.

Lansard, B., 2005. Distribution et remobilisation du plutonium dans les sédiments du prodelta du Rhône (Méditerranée Nord-Occidentale). Thèse de doctorat, pp. 180.

Lansard, B., Grenz, C., Charmasson, S., Schaaff, E., Pinazo, C., 2006. Potential plutonium remobilisation linked to marine sediment resuspension: first estimates based on flume experiments. *Journal of Sea Research*, 55, 74-85.

Law, B.A., Hill, P.S., Milligan, T.G., Curran, K.J., Wiberg, P.L., Wheatcroft, R.A., 2008. Size sorting of the fine-grained sediments during erosion: results from the western Gulf of Lions. *Continental Shelf Research*, 28 (15), 1935-1946.

Maillet, G., Vella, C., Berné, S., Friend, P., Amos, C., Fleury, T., Normand, A., 2006. Morphological changes and sedimentary processes induced by the December 2003 flood event at the present mouth of the Grand Rhône River (Southern France). *Mar. Geol.*, 234, 159-177.

Maréchal, J.C., Ladouche, B., Dörflinger, N., 2006. Role of karst system in the genesis of flash flood events in the Nîmes city. EGU 2006, Geophysical Research Vol.8, 06173, 2006.

Milligan, T.G., Hill, P.S., Law, B.A., 2007. Flocculation and the loss of sediment from the Po River plume. *Continental Shelf Research*, 27, 309-321.

Miralles, J., Arnaud, M., Radakovitch, O., Marion, C., Cagnat, X., 2006. Radionuclide deposition in the Rhône River Prodelta (NW Mediterranean Sea) in response to the December 2003 extreme flood. *Mar. Geol.*, 234, 179-189.

Miralles, J., Radakovitch, O., Aloisi, J.C., 2005.  $^{210}\text{Pb}$  sedimentation rates from the Northwestern Mediterranean margin. *Mar. Geol.*, 216, 155-167.



- 1  
2  
3  
4  
5 Monaco, A., Biscaye, P.E., Pocklington, R., 1990. France-JGOFS, ECOMARGE, Particle fluxes and  
6 ecosystem response on a continental margin: the mediterranean experiment. *Continental Shelf*  
7 *Research*, 10, 9-11.  
8  
9 Monaco, A., Durrieu de Madron, X., Radakovitch, O., Heussner, S., Carbone, J., 1999. Origin and  
10 variability of downward biogeochemical fluxes on the Rhône continental margin (NW  
11 Mediterranean). *Deep Sea Research I* 46, 1483-1511.  
12  
13 Moore, W.S., DeMaster, D.J., Smoak, J.M., McKee, B.A., Swarzenski, P.W., 1995. Radionuclide  
14 tracers of sediment-water interactions on the Amazon shelf. *Continental Shelf Research*, 16, 5/6,  
15 645-665.  
16  
17 Naudin, J.J., Cauwet, G., Chrétiennot-Dinet, M.J., Deniaux, B., Devenon, J.L., Pauc, H., 1997. River  
18 discharge and wind influence upon particulate transfer at the land-ocean interaction : case study of  
19 the Rhône River plume. *Estuar. Coast. Shelf Science*, 45, 303-316.  
20  
21 Nittrouer, C.A., De Master, D.J., McKee, B.A., Cutshall, N.H., Larsen, I.L., 1983/1984. The effect of  
22 sediment mixing on Pb-210 accumulation rates for the Washington continental shelf. *Mar. Geol.*,  
23 54, 201-221.  
24  
25 Nittrouer, C.A., De Master, D.J., 1986. Sedimentary processes on the Amazon continental shelf: past,  
26 present and future research. *Cont. Shelf Research* 6, 5-30.  
27  
28 Nittrouer, C.A., Kuelh, S.A., Sternberg, R.W., Figueiredo, Jr A.G., Faria, L.E.C., 1995. An  
29 introduction to the geological significance of sediment transport and accumulation on the Amazon  
30 continental shelf. *Mar. Geol.*, 125, 177-192.  
31  
32 Palanques, A., Durrieu de Madron, X., Puig, P., Fabres, J., Guillén, J., Calafat, A, Canals, M.,  
33 Heussner, S., Bonnin, J., 2006. Suspended sediment fluxes and transport processes in the Gulf of  
34 Lions submarine canyons. The role of storms and dense water cascading. *Mar. Geol.*, 234 (1-4),  
35 43-61.  
36  
37 Palinkas, C.M., Nittrouer, C.A., 2007. Modern sediment accumulation on the Po shelf, Adriatic Sea.  
38 *Continental Shelf Research*, 27, 489-505.  
39  
40  
41  
42  
43  
44  
45  
46  
47  
48  
49  
50  
51  
52  
53  
54  
55  
56  
57  
58  
59  
60  
61  
62  
63  
64  
65

- 1  
2  
3  
4  
5  
6  
7  
8  
9  
10  
11  
12  
13  
14  
15  
16  
17  
18  
19  
20  
21  
22  
23  
24  
25  
26  
27  
28  
29  
30  
31  
32  
33  
34  
35  
36  
37  
38  
39  
40  
41  
42  
43  
44  
45  
46  
47  
48  
49  
50  
51  
52  
53  
54  
55  
56  
57  
58  
59  
60  
61  
62  
63  
64  
65
- Palinkas, C.M., Nittrouer, C.A., Wheatcroft, R.A., Langone, L., 2005. The use of  $^7\text{Be}$  to identify event and seasonal sedimentation near the Po River delta, Adriatic Sea. *Mar. Geol.* 222-223, 95-112.
- Pauc, H., 2005. Formation of the Aude, Orb and Herault prodeltas and their characterisation using physicochemical and sedimentological parameters. *Mar. Geol.*, 222-223, 335-343.
- Pont, D., Simonnet, J.P., Walter, A.V, 2002. Medium-terms changes in suspended sediment delivery to the ocean: consequences of catchment heterogeneity and river management (Rhône river, France). *Estuar. Coast. Shelf Sci.* 54, 1-18.
- Radakovitch, O., Charmasson, S., Arnaud, M., Bouisset, P., 1999.  $^{210}\text{Pb}$  and caesium accumulation in the Rhône delta sediments. *Estuar. Coast. Shelf Sci.* 48, 77-92.
- Radakovitch, O., Roussiez, V., Ollivier, P., Ludwig, W., Grenz, C., Probst, J.L., 2008. Input of particulate heavy metals from rivers and associated sedimentary deposits on the Gulf of Lions continental shelf. *Estuar. Coast. Shelf Sci.*, 77 (2), 285-295.
- Rolland, B., 2006. Transfert des radionucléides artificiels par voie fluviale : conséquences sur les stocks sédimentaires rhodaniens et les exports vers la Méditerranée. Thèse de doctorat, pp. 280.
- Roussiez, V., Aloisi, J.C., Monaco, A., Ludwig, W., 2005. Early muddy deposits along the Gulf of Lions shoreline: a key for a better understanding of the land-to-sea transfer of sediments and associated pollutant fluxes. *Mar. Geol.*, 222-223, 345-358.
- Roussiez, V., 2006. Les éléments métalliques: traceurs de la pression anthropique et du fonctionnement hydro-sédimentaire du Golfe du Lion. Thèse de doctorat à l'Université de Perpignan, 130 pp.
- Sabatier, P., Maillet, G., Provansal, M., Fleury, T.J., Suanez, S., Vella, C., 2006. Sediment budget of the Rhône delta shoreface since the middle of the 19<sup>th</sup> century. *Mar. Geol.*, 234, 143-157.
- Serrat, P., Ludwig, W., Navarro, B., Blazi, J.L., 2001. Variabilité spatio-temporelle des flux de matières en suspension d'un fleuve côtier méditerranéen : la Têt (France). *Earth and Planetary Sciences*, 333, 389-397.
- Sommerfield, C.K., Nittrouer, C.A., 1999. Modern accumulation rates and a sediment budget for the Eel shelf: a flood-dominated depositional environment. *Mar. Geol.*, 154, 227-241.

- 1  
2  
3  
4  
5  
6  
7  
8  
9  
10  
11  
12  
13  
14  
15  
16  
17  
18  
19  
20  
21  
22  
23  
24  
25  
26  
27  
28  
29  
30  
31  
32  
33  
34  
35  
36  
37  
38  
39  
40  
41  
42  
43  
44  
45  
46  
47  
48  
49  
50  
51  
52  
53  
54  
55  
56  
57  
58  
59  
60  
61  
62  
63  
64  
65
- Soulsby, R.L., 1997. Dynamics of marine sands. A manual for practical applications. 249 pp., Thomas Telford, London.
- Sternberg, R.W., Cacchione, D.A., Paulson, B., Kineke, G.C., Drake, D.E., 1996. Observations of sediment transport on the Amazon subaqueous delta. *Continental Shelf Research* 16, 697-715.
- Swart, D.H., 1974. Offshore sediment transport and equilibrium beach profiles. Delft Hydraulics Laboratory publication, 131.
- Syvitski, J.P.M., Kettner, A.J., Corregiari, A., Nelson, B.W., 2005. Distributary channels and their impact on sediment dispersal. *Mar. Geol.*, 222-223, 75-94.
- Tessier, C., 2006. Caractérisation et dynamique des turbidités en zone côtière : l'exemple de la région marine Bretagne Sud. Thèse de doctorat à l'Université de Bordeaux I n°3307. 400p.
- Thill, A., Moustier, S., Garnier, J.M., Estournel, C., Naudin, J.J., Bottero, J.Y., 2001. Evolution of particle size and concentration in the Rhône river mixing zone: influence of salt flocculation. *Continental Shelf Research*, 21 (2127-2140).
- Thomas, A.J., 1997. Input of artificial radionuclides to the Gulf of Lions and tracing the Rhône influence in marine surficial sediments. *Deep Sea Research II*, 44, 577-595.
- Tolman, H.L., 2002a. User manual and system documentation of WAVEWATCH-III version 2.22. Tech. report 222, NOAA/NWS/NCEP/MMAB.
- Wheatcroft, R.A., Drake, D.E., 2003. Post-depositionnal alteration and preservation of sedimentary event layers on continental margins, I. The role of episodic sedimentation. *Mar. Geol.*, 199, 123-137.
- Weaver, P.P.E., Canals, M., Trincardi, F., 2006. EUROSTRATAFORM: special issue of *Marine Geology*. *Mar. Geol.*, 234, (1-4), 1-2.
- Zuo, Z., Eisma, D., Gieles, R., Beks, J., 1996. Accumulation rates and sediment deposition in the northwestern Mediterranean. *Deep Sea Research*, 44, 3-4, 597-609.

Fig. 1: Bathymetric map of the Grand Rhône River mouth. Dots represent the cores sampling stations.

Fig. 2: Water flows of upstream (a) and downstream (b) Rhône tributaries during the floods of Nov. and Dec. 2006. (CNR).

Fig. 3 : ADCP data recovered in the whole water column close to the Roustan Est buoy (current directions in degrees (a); current velocity in  $\text{cm s}^{-1}$  (b); turbidity in dB (c)), sedimentation evolution in cm next to the Roustan Est buoy (d), winds direction and intensity in  $\text{m s}^{-1}$  (e), Rhône River flow in  $\text{m}^3 \text{s}^{-1}$  measured in Beaucaire (f), swell direction in degrees (spots) and height in m (curve) at the Rhône River mouth (g).

Fig. 4: Current velocity in  $\text{cm s}^{-1}$  and direction (sticks) in the whole water column from 1.5 mab near the Roustan Est buoy.

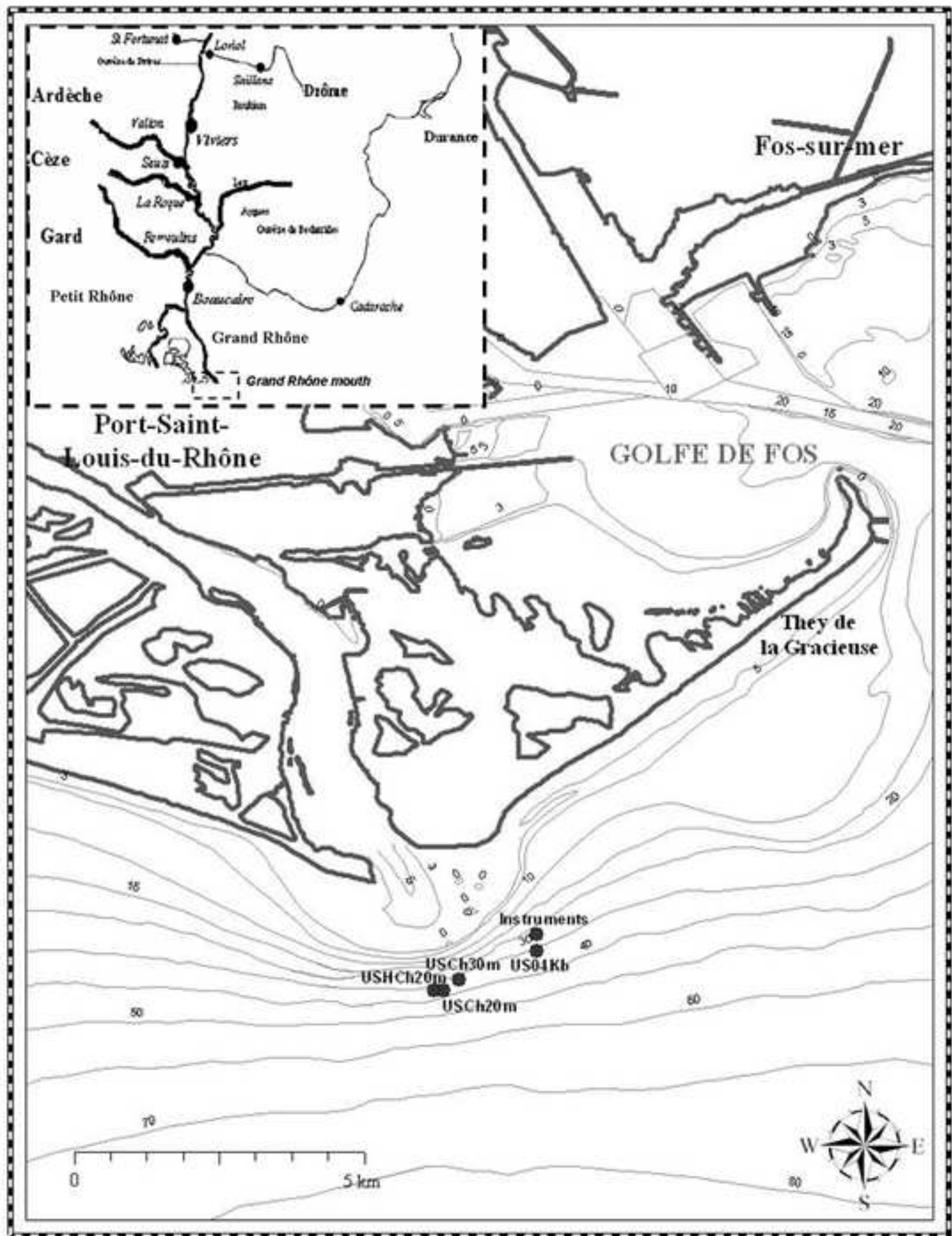
Fig. 5: Volumic retrodiffusion index (BBI) in dB 1.5 m above the bottom (a), bottom shear stress in  $\text{N m}^{-2}$  due to: the currents (b), the waves (c), the currents and the waves (d).

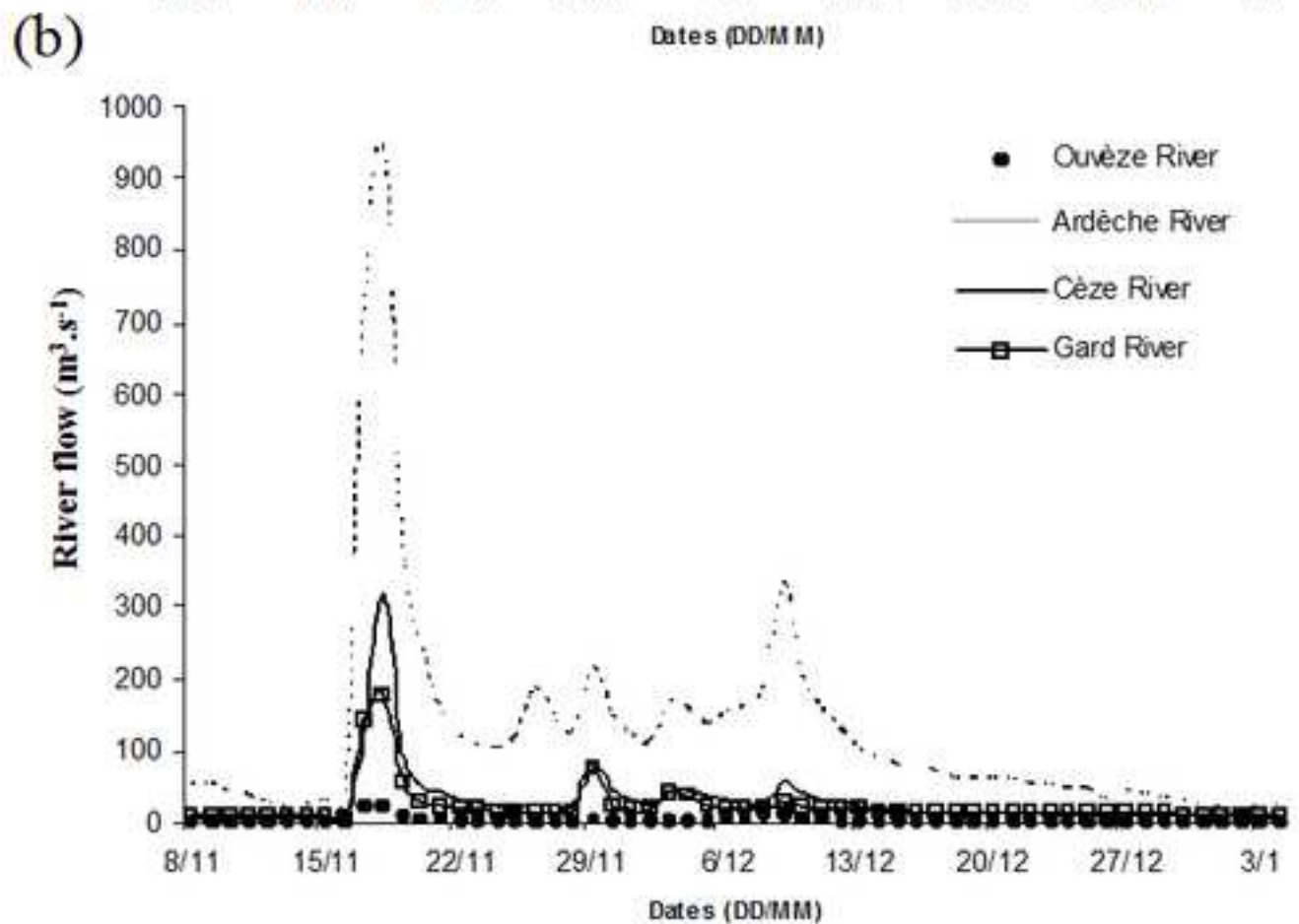
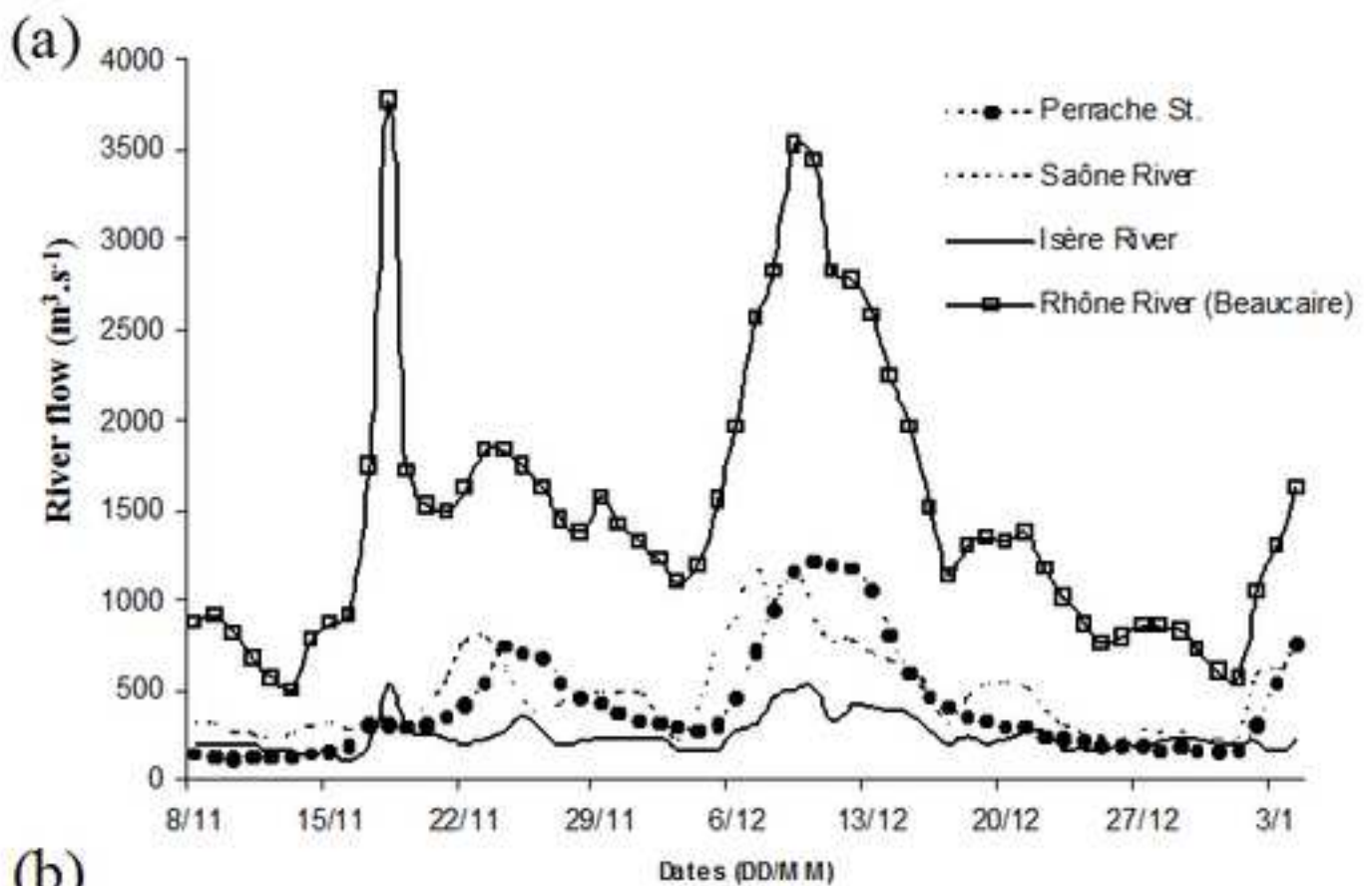
Fig. 6: Rhône River flow in  $\text{m}^3 \text{s}^{-1}$  between the end of the altimeter record and the core sampling time.

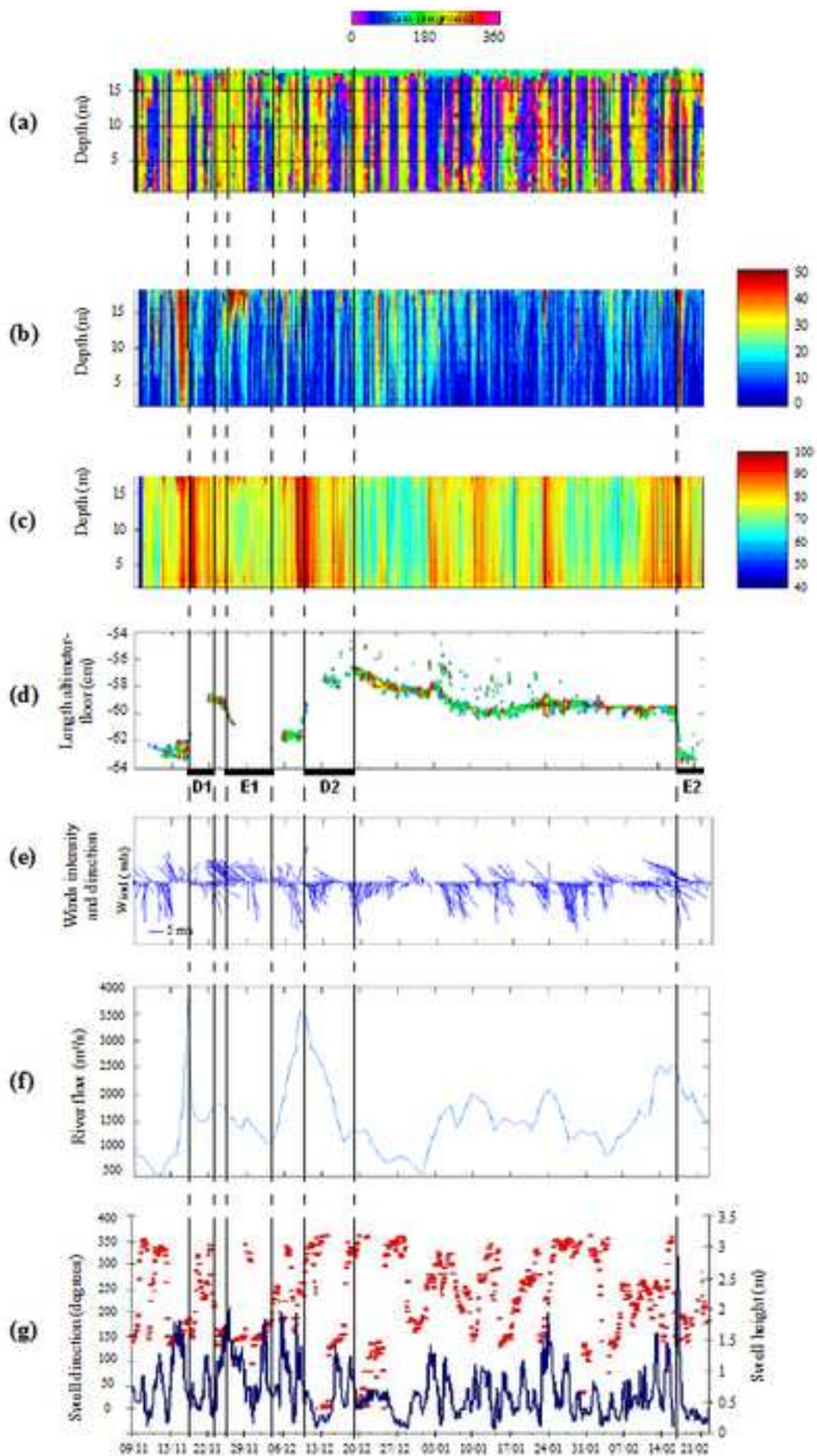
Fig. 7: Mean grain sizes in micrometers (top) and grain-size vertical distribution (bottom) in the USHC20, USC30, USC20 and US04Kb cores sampled during the CARMEX campaign.

Fig. 8: Vertical radionuclides activities ( $^{137}\text{Cs}$ ,  $^7\text{Be}$ ,  $^{234}\text{Th}$ ,  $^{210}\text{Pb}$ ) in  $\text{Bq kg}^{-1}$  dry weight in the USHC20 (left), USC30 (center) and USC20 (right) cores sampled during the CARMEX campaign.

CM-Fig. 1  
[Click here to download high resolution image](#)







CM-Fig. 4  
[Click here to download high resolution image](#)

